MASTER'S THESIS

ENERGY EFFICIENCY IN LORAWAN

Author   Junnaid Iqbal

Supervisor   Assist. Prof. Dr. Hirley Alves

Second Examiner   Assist. Prof. Konstantin Mikhaylov

June   2020

ABSTRACT

Low-power wide-area networks (LPWANs) are emerging rapidly as a fundamental Internet of Things (IoT) technology because of features like low-power consumption, long-range connectivity, and the ability to support massive numbers of users. With its high growth rate, Long Range (LoRa) is becoming the most adopted LPWAN technology. Sensor nodes are typically powered by batteries, and many network applications, which expect end-devices to operate reliably for a prolonged time. Each sensor node or actuator consumes a distinct current for a different period of time, depending on its operational state. To model a self-sufficient sensor nodes network, it is of the utmost importance to investigate the energy consumption of class-A end-devices in a LoRa Wide Area Network (LoRaWAN) with the impact of respective physical and MAC layers. Several latest published research works have analyzed the energy consumption model of a sensor node in different transmission (confirmed or unconfirmed) modes and also examined the network performance of LoRaWAN under uplink outage probabilities. This research work investigates the energy cost of the LoRaWAN, deploying hundreds of sensor nodes to transmit information messages. The proposed scheme is evaluated by considering the average power consumption of end-device powered by 2400 mAh battery. Furthermore, the energy efficiency of an unconfirmed transmission network is examined to provide the optimal number of sensor nodes for each spreading factor.

Keywords: LoRaWAN, stochastic geometry, Internet of Things, performance evaluation, energy consumption.

TABLE OF CONTENTS

FOREWORD

The focus of this research work is related to the study Energy Efficiency in LoRaWAN Network. The thesis work was undertaken at the Center for Wireless Communication (CWC) of the University of Oulu, Finland, and financially supported by MOSSAF project.

Oulu, 4th June, 2020

Junnaid Iqbal

LIST OF ABBREVIATIONS AND SYMBOLS

Acronyms

ACK	Acknowledgment
ADR	Adaptive Data Rate
AES	Advanced Encryption Standard
AS	Application Server
AWGN	Additive White Gaussian Noise
BER	Bit error rate
CDF	Cumulative Distribution Function
CDMA	Code Division Multiple Access
CF	Carrier Frequency
CR	Coding Rate
CSS	Chirp Spread Spectrum
DSSS	Direct Sequence Spread Spectrum
ECC	Error correction code
ED	End-devices
FEC	Forward Error Correction
FHDR	Frame Header
FRMPayload	Frame Payload
FCtrl	Frame Controller
GSM	Global System for Mobile Communication
GW	Gateway
IoT	Internet of Things
LoRaWAN	LoRa Wide Area Network
LPWAN	Low Power Wide Area Network
LTE	Long-term Evolution
MAC	Media Access Control
MCS	Modulation and Coding Scheme
MHDR	MAC Header
MIC	Message Integrity Check
MIMO	Multiple-Input Multiple-Output
MTC	Machine-type Communications
MType	Message Type
NS	Network Server
OFDMA	Orthogonal frequency-division Multiple Access
PER	Packet Error Rate
PPP	Poisson point process
QPSK	Quadrature Phase Shift Keying
QR	Quick Response
RFID	Radio-frequency identification
SIR	Signal-to-Interference ratio
SISO	Single-Input Single-Output
SNR	Signal-to-Noise ratio
ToA	Time-on-Air
UNB	Ultra-Narrow Band

Symbols

DR	Data Rate
f	Carrier Frequency
SF	Spreading Factor
RX_1	First Receiver Window
RX_2	Second Receiver Window
$\mathcal{N}$	Variance of AWGN
$\bar{N}$	Number of nodes
R	Radius of coverage area
R_{l_i}	Width of SF annulus
q_{SF}	SNR reception threshold
$\mathcal{P}_1$	Transmit power of end-device
$\wp_c$	Average Coverage probability
P_{Ack}	Power Consumption for Acknowledged Transmission
$\bar{P}_{Ack}$	Avg. Power Consumption for Acknowledged Transmission
P_{unAck}	Power Consumption for Unacknowledged Transmission
$\bar{P}_{unAck}$	Avg. Power Consumption for Unacknowledged Transmission
p	Density of PPP
$\bar{n}$	Preamble length
RX_{1OFF}	First receiver window offset
BW	Bandwidth
T_S	Symbol duration
R_b	Bit Rate
CRC	Cyclic Redundancy Check
PL	Physical Payload Length
$ACK_{Timeout}$	Acknowledgment Timeout
$g(d_i)$	Path loss attenuation at transmission distance d_i
η	Path loss exponent
λ	Wavelength
NF	Noise figure of the receiver
$|h_1|^2$	Squared envelop of the channel coefficient
d_1	Distance between desired end-device and gateway
H_1	Connection Probability
Q_1	Capture Probability
H_1Q_1	Coverage Probability
l_i, l_{i+1}	Inner and Outer radii of i-th annulus, respectively
T_{active}	Sum of all transmission states except sleep state
LS	Link Success
EC	Energy Cost
EE	Energy Efficiency
$\wp_{outage}$	Average Outage Probability

1 INTRODUCTION

The Internet of Things (IoT) promises the integration of smart objects, sensors, internet protocols, and wireless technologies, etc to share information and communicate among themselves using defined protocols [1]. The IoT is about to remove the limitation of the internet to merely computers and smartphones and expand it to a set of other aspects of our surroundings, i.e., building automation, weather monitoring, process controlling, etc. Some of the key features of IoT include the ability of smart objects to gather information comprehensively, transmit the required information in a secure mechanism, and do intelligent post-processing on the gathered data. The usage of Radio-frequency identification (RFID), Quick Response (QR) codes, and wireless technology are paving ways to enable intercommunication between humans, people to devices, and devices to other devices. Such applications are enablers of many vital operations in industrial environments [2], smart parking systems [3], Internet of Health things (IoHT) [4], augmented maps, and smart cars [5]. According to Statista report [6], there will be over 75 billion smart IoT devices worldwide by the end of 2025.

Machine-type communications (MTC) is a paradigm that enables devices to exchange information autonomously and perform actions without human interference. MTC technologies can connect devices to virtually anything within a single network. These devices integrate meters in a smart grid, commerce, energy sector, and housing. Power line communications (PLC) or the Internet of Things (IoT) using wireless communications in the industrial domain are becoming highly mainstream. The transformation from traditional wired infrastructure to wireless communication has enabled more devices, applications, and services to communicate among themselves. Such communication is one enabler of IoT and plays a critical role in the successful deployment.

Sensor nodes empower the IoT paradigm by the transformation of wireless connectivity in a regular and harsh environment. For such reasons, nodes must operate with technologies having characteristics of large-scale network infrastructure with low power consumption. These constraints assist in the introduction of the Low Power Wide Area Network (LPWAN). As of 2012, LPWAN did not exist but with its introduction, LPWAN technologies provided futuristic communication that ensures the long-range with low power consumption and low-cost deployment [7]. It was particularly designed for such applications that require few messages per day to be sent in a long radio range. Within this context, SigFox, LoRaWAN, and NB-IoT are the most popular technologies.

1.1 Features of LPWAN Techniques

The fame behind the LPWAN technologies stands for their ability to ensure long range transmission to a massive number of low powered number of devices connected with low cost solutions. According to [8], the key features of LPWAN are Long Range, Ultra Low-power Operations, Low Cost, and Scalability. They are detailed as follows:

1.1.1 Long Range

LPWAN technologies assist in offering wide area coverage with good signal propagation even in unfavorable indoor conditions. End-devices can communicate with a base station at a distance up to tens of kilometers. Different characteristics are used to achieve this goal.

1. **Sub-GHz Band:** The use of a sub-GHz band offers reliable communication at a favorable power budget. Low-frequency signal has advantages in terms of attenuation and multipath fading because of obstacles or dense surfaces. In addition, these frequencies are less congested as most of the popular wireless technologies like Wi-Fi, Bluetooth, and ZigBee operate on 2.4 GHz.

2. **Modulation:** Modulation techniques like Narrow band and Spread spectrum are utilized to achieve a link budget of 150 ± 10 dB for LPWAN technologies. Higher data rate and low modulation rate by the physical layer results in an increase in energy per transmitted bit. As of this, the receiver can easily detect and decode the weakened signals. In Narrowband modulations, each carrier is assigned with a narrow frequency band to efficiently share the spectrum over multiple links. The noise level is minimal inside a single narrowband channel. Thus, frequency despreading is not desired at the receiver end to correctly decode input data stream from carriers. This leads to the design of simple and inexpensive transceivers. NB-IoT is an example of said modulation technology. SigFox uses ultra-narrow band (UNB) having carrier signal width as low as 100 Hz bandwidth, resulting in a reduction of noise level and inclusion of more end-devices. Spread-spectrum modulation spreads the narrowband transmission signal over the broad frequency band without altering the power density. This shows more resilience to interference and jamming attacks. Different transmission channels and orthogonal sequences can assist in increasing network capacity. LoRa technology is operated on the principle of Chirp Spread Spectrum (CSS).

1.1.2 Ultra Low-power Operations

It is necessary for a technology to have ultra-low power consumption to tap into the business of IoT/MTC devices, which operates on batteries. The main design techniques LPWANs to achieve it are:

1. **Topology:** LPWAN technologies follow the star topology to overcome the congestion and deployment cost faced by the network deployed on mesh configuration. End-devices directly communicate with the base station, in a star topology, to prevent the requirement of relays and gateways. In contrast with mesh topology, the precious energy of nodes does not waste in listening to other devices for relaying the traffic. Few LPWAN technologies follow tree and mesh topologies, so they feature complex protocols.

2. **Duty Cycle:** Power efficient operation is only possible to turn off power-hungry components of IoT devices. Duty cycle restriction helps the LPWAN technologies only to send or receive data when it is required. To this effect, power hungry

components i.e., transceivers, are mostly switched off during the life cycle of the network. If the application needs to send data over uplink communication, then end-device only wake up for transmission. In addition, end-device only listens when the base station transmits the data in downlink mode. Regional guidelines are in place for a transmitter to define the time limit to occupy the channel. Some famous standard developing organizations are European Telecommunication Standard Institute (ETSI) [9] and Institute of Electrical and Electronics Engineering (IEEE) [10].

3. **Medium Access Control (MAC):** Multiple LPWAN technologies i.e., SigFox and LoRaWAN use ALOHA-like protocol as a random access MAC to communicate with the gateway without the need for sensing the carrier. The reason is to keep the transceiver design simple and cost-efficient.

4. **Complexity:** Complex tasks are operated at the base station, which provides the nodes an opportunity to send or receive information through multiple radio channels or orthogonal signals. Furthermore, embedding smart tasks in the back-end systems can give benefit to end-devices in terms of reliability and energy efficiency. The notable operations are modification in communication parameters (data rate, modulation parameters), fair resource allocation, and support for end-devices to shift between multiple base stations.

1.1.3 Low Cost

One of the reasons behind the popularity of LPWAN technologies concerning commercial success is cost efficiency, keeping the hardware price up to a few dollars [11]. This enables technologies to provide services to multiple applications and compete with cellular networks.

1. **Hardware:** LPWAN transceivers have less footprint, as they process less complex waveform and also optimize to tolerate clock drifts. It enables transceivers to minimize peak data rate, memory size, and complexity of hardware design.

2. **Development Infrastructure:** A single LPWAN base station connects with hundreds of end-devices distributed over a couple of miles, considerably lower the cost of dense infrastructure and network operations.

1.1.4 Scalability

LPWAN technologies must cope with the immense number of nodes transmitting low data volume. Several methods are considered, which helps in the resolution of scalability problems.

1. **Diversity Methods:** Diversity in terms of time, space, and channel is utilized to accommodate an enormous number of devices. The exploitation of diversity is accomplished by the assistance of the base station or gateway. Furthermore, communication between the end-device and gateway is made resilient from interference and channel noise by employ multiple channels and redundant transmission.

2. **Channel Selection, Data Rate, and Transmit Power Control:** Adaptive Channel selection, Data Rate, and optimization of Transmit Power provide the LPWAN network to scale up to multiple connected devices. Therefore, it is required to optimize the individual link for reliability and energy efficiency. Adapting modulation schemes with better channel selection will improve the link quality along with coordination among end-device and gateway.

1.2 LPWAN Technologies

In this section, different proprietary technologies e.g. SigFox, LoRaWAN, and NB-IoT are highlighted.

1.2.1 SigFox

SigFox offers LPWAN solutions deployed across different regions in unlicensed sub-GHz bands. For instance, Sigfox operates in Europe, North American, and Asia with 868 MHz, 915 MHz, and 433 MHz, respectively.

Network operators deploy the Sigfox solution by equipping base stations with cognitive software-defined radios directly connected with back-end servers using the IP network. In uplink communication, end-devices communicate with the base station through Binary Shift Keying (BPSK) modulation in a narrowband of 100 Hz with a data rate of 100 bps. Consequently, the utilization of UNB in the sub-GHz spectrum results in better frequency band usage having a low noise level [12]. This leads to higher receiver sensitivity and low power consumption. Further, Sigfox early used for uplink communication, but later it improved into the bidirectional transmission. The number of messages over uplink transmission is confined to 140 having 12-byte message size by regional regulations [13]. Nevertheless, downlink messages are only limited to 4 messages per day, and thereby the base station could not acknowledge every uplink message. The payload size of downlink message is 8 bytes. Without acknowledgment, the reliability of uplink transmission is enhanced by message, time diversity, and retransmission. The base station scans all the frequency channels, while node transmits data messages three times through distinct frequency channels. This transmission method reduces the complexity and cost of the end-device.

1.2.2 NB-IoT

NB-IoT is narrow band IoT technology, which coexists in LTE and GSM under licensed frequency bands. It occupies a bandwidth of 200 kHz and following operation modes are available, **Stand alone:** which considers the utilization of current GSM frequency band, **Guard Band:** make use of idle resource block in guard band of LTE carrier, and **In-Band:** employ resource block in LTE carrier. The operation modes of NB-IoT are demonstrated in Figure 1

In-Band Operation *Guard Band Operation* *Stand Alone Operation*

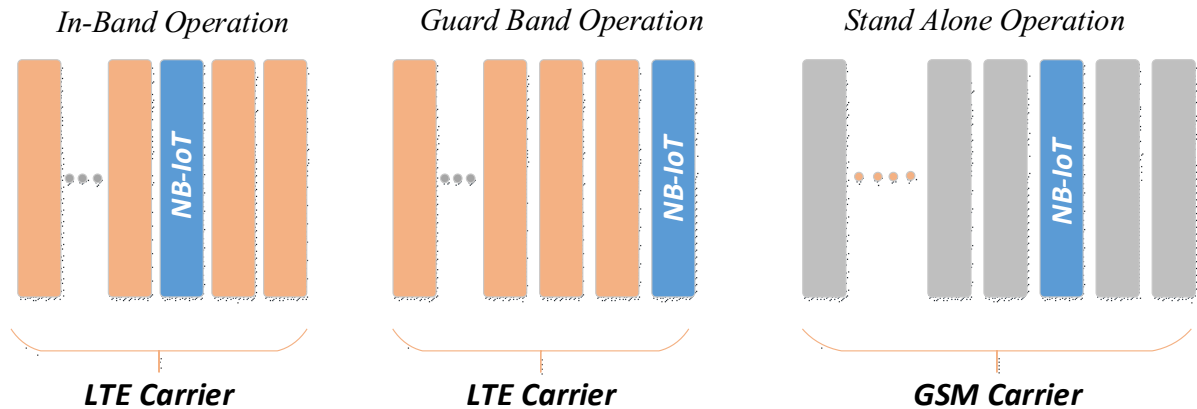**LTE Carrier** **LTE Carrier** **GSM Carrier**

Figure 1. Operation Modes of NB-IoT.

NB-IoT communication protocols are based on the principle of LTE, so it can be beneficial to IoT devices and their applications. Up to 100k devices can be connected with NB-IoT carriers. It employs restricted BPSK and QPSK modulation [14]. Frequency Division Multiple Access (FDMA) for transmitting data from node to base station up to 20 kbps throughput. Orthogonal Frequency Division Multiple Access (OFDMA) is also employed for downlink communication at a maximum throughput of 200 kbps having a payload size up to 1600 bytes [15].

1.2.3 LoRaWAN

LoRa is a spread spectrum technology introduced by the Semtech and standardized by the LoRa-Alliance in 2015. This LPWAN technology modulates the signal through the chirp spread spectrum (CSS) under sub-GHz band to provide bidirectional communication. Further, it makes the modulated signal resilient to interference and channel noise. Transmitter renders the chirp signal to alter their frequency with time irrespective of varying phase difference among symbols. The receiver can easily decode the modulated chirp signal if the frequency change is slow enough, which results in better energy per chirp symbol. Forward Error Correction (FEC) also employed to improve receiver sensitivity. LoRa provides the communication range up to 15 km and 30 km over ground and water respectively [16].

LoRaWAN is an open standard network stack that exploits characteristics of LoRa physical layer. The main aim behind its development is to provide sensors with an opportunity to exchange data frames with a server with minimum data rate and comparatively distinct time duration among transmissions (i.e., one transmission per 1 hour or 24 hours). Network architecture is deployed in a star-of-stars topology wherein end-devices (ED) are connected with network servers (NS) through the gateway (GW).

LoRaWAN modifies the bitrate in accordance with the available channel quality. It utilizes the feature of SF to adapt among the robustness of modulated signal and bitrate. When a sensor node encounters a poor link quality, LoRaWAN increases SF for the modulated signal to be transmitted over long range. Though bitrate would be low in this

scenario. This alteration of data rate is managed by LoRaWAN parameter (DR) and in EU it varies among $DR0$ ($SF12$, low bitrate) to $DR5$ ($SF7$, high bitrate).

1.2.4 Comparison of LPWAN Technologies

It is essential to choose a suitable LPWAN technology that will be feasible for IoT applications. The technical features of each technology are outlined in Table 1.

Sigfox and LoRaWAN utilize license-free sub-GHz bands and asynchronous communication properties. This helps to counter interference and multipath fading. NB-IoT utilizes licensed spectrum to provide QoS at the expense of high cost. In terms of lifetime, NB-IoT devices have less operating life because of synchronous communication of its end-devices and OFDM/FDMA access modes, which require peak current [17].

The standardization of NB-IoT was released in 2016 and still in the rollout phase to deploy its network around the globe. In contrast, the deployment model of other LPWAN technology is mature, and amongst all, currently, LoRaWAN technology has been deployed in more than 100 countries [18]. Furthermore, LoRaWAN can provide local network deployment, public network deployment, and also a hybrid operating model where local LoRaWAN network can integrate with a public network via base stations.

Table 1. Technical Specification of LPWAN Technologies

	SigFox	**LoRa**	**NB-IoT**
Modulation	BPSK	CSS	QPSK
Frequency	Sub-GHz ISM • EU 868 MHz • US 902 MHz	Unlicensed ISM • EU 868 MHz • US 915 MHz	Licensed LTE Frequency bands
Data Rate	• 100 bps (UL) • 600 bps (DL)	$0.3 - 50$ kbps	200 kbps
Range	• 10 km (Urban) • 50 km (Rural)	• 5 km (Urban) • 15 km (Rural)	• 1 km (Urban) • 10 km (Rural)
MCS	No	Yes	No
Auth. & Encrypt.	Encryption not supported	AES 128b	LTE encryption [19]

1.3 Thesis Contribution

The main research goal of this thesis work focuses on the energy efficiency of the LoRaWAN network that considers hundreds of concurrently transmitting end-devices uniformly distributed around the gateway in a radius of several kilometers. We study two distinct scenarios, wherein one case a sensor node sends information to gateways without considering outage probability caused by the imperfect channel behavior. The average power consumption of end-device is examined when it does not retransmit the message. The second scenario deals with the retransmission of message several times

over the uplink radio channel and expects an acknowledgment from the gateway in one of two receive windows. Correspondingly, average power consumption is also reviewed for the latter approach. In addition, we have investigated the performance of uplink communication in the presence of outage conditions faced by the end-devices. These measurements help to find the relationship between energy consumption and interference level of LoRaWAN network. The average power consumption of a sensor node in distinct transmission modes assists in determining the operating lifetime. This research work contributes towards measuring the energy cost of massive uniformly distributed end-devices in LoRaWAN. Furthermore, Energy efficiency of the network is considered depending on the average coverage probability of providing an optimal number of sensor nodes for distinct increasing distance from the gateway.

1.4 Thesis Outline

The remainder of thesis work is structured as follows. In Chapter 2, we describe the general architecture of LoRaWAN, reviewing main parameters of physical and MAC layers, and also discuss the related work in modeling the energy performance of end-devices in sensor networks. Chapter 3 introduces the system model which deals with uplink outage probabilities and two distinct transmission modes (Unacknowledged and Acknowledged). Numerical results and evaluation are present in Chapter 4 and our conclusion of research work is provided in Chapter 5.

2 LORAWAN OVERVIEW AND RELATED WORK

In this chapter, several characteristics of LoRaWAN and related work are presented. Initially, we start with protocol architecture along with physical and MAC layer, defining the procedure and key parameters in transmitting information based on LoRa technology.

2.1 LoRaWAN Overview

LoRa refers to 'Long Range,' which is a long range technology having low power consumption. This technology aims at increasing the lifetime of battery-powered sensors with minimal cost. LoRa usually described as having two layers

1. **Physical Layer:** Chirp Spread Spectrum (CSS) radio modulation process is used to communicate among end-device and gateway while retaining LoRa characteristics i.e., low power with maximum communication range.

2. **MAC Layer:** LoRa MAC layer protocol is known as LoRaWAN, which uses multicast networking protocol. It defines the set of rules for radio waves to access LoRaWAN gateway to perform channel operations.

The LoRa physical layer is a proprietary technology of Semtech while LoRaWAN is an open standard by LoRa-Alliance.

2.1.1 LoRa Physical Layer

Continuous variation of frequency over time to encode data makes CSS modulation resistant against the Doppler effect. Although the frequency offset between transmitter and receiver reaches 20% of total bandwidth without effecting on the decoding performance. Therefore, crystal placed in a transmitter does not require to have maximum accuracy, which reduces the manufacturing cost of LoRa transmitter. There are the following several essential configuration parameters of LoRa radio.

- **Carrier Frequency (CF):** It is the frequency used for the transmission of a message from node to gateway. LoRa operates at unlicensed frequency ISM bands in Europe and the U.S. at 863-870 MHz and 915 MHz, respectively [12, 20].

- **Spreading Factor (SF):** Number of chirps per symbol is called Spreading Factor. LoRa has 6 SFs i.e. 7, 8, 9, 10, 11, 12. Higher SFs allow larger coverage areas; however, as a drawback, they reduce the data rate and increase the time-on-air (ToA) of LoRa packets [21]. One symbol has 2^{SF} chirps for the overall frequency band.

- **Bandwidth (BW):** There are three bandwidth options for LoRa communication i.e., 125 kHz, 250 kHz, and 500 kHz. 125 kHz is normally used for the 863-870 MHz frequency band. For the rapid transmission, it is better to use 500 kHz bandwidth, and if a long coverage area is required, 125 kHz is recommended.

Table 2. Semtech SX1276, Sensitivity of LoRa Receiver (dBm)[22]

BW	Spreading Factor					
	$SF7$	$SF8$	$SF9$	$SF10$	$SF11$	$SF12$
125 kHz	-126.50	-127.25	-131.25	-132.75	-134.50	-133.25
250 kHz	-124.25	-126.75	-128.25	-130.25	-132.75	-132.25
500 kHz	-120.75	-124.00	-127.50	-128.75	-128.75	-133.25

The relationship among duration of symbol T_S, bandwidth and spreading factor is provided in Equation 1

$$T_S = \frac{2^{SF}}{BW} \, . \tag{1}$$

- **Coding Rate (CR):** Coding rate expression is $CR = \frac{4}{4+n}$ where $n \in \{1,2,3,4\}$. Lower coding rate provides higher time-on-air (ToA) to transmit information. The LoRa modulation bit rate R_b is defined as [21]

$$R_b = \frac{4}{4+n} \frac{BW}{2^{SF}} \, . \tag{2}$$

These parameters have an adverse impact on receiver sensitivity. Table 2 summarizes the relationship between BW, SF, and Receiver Sensitivity. An increase in bandwidth will lower the decoder sensitivity, although the spreading factor has a proportional relationship with receiver sensitivity. The decrease in code rate will help to reduce Packet Error Rate (PER) against interference. For instance, a data message transmitted with a 4/8 code rate is more resilient against channel implications as compared to a code rate of 4/5.

Physical Layer Message Format

The physical layer frame format is defined and embedded in Semtech manufactured transceivers. Bandwidth and spreading factor remain the same for a message frame. LoRa physical layer message consists of a preamble, physical header, physical header Cyclic redundancy check, physical payload and cyclic redundancy check for error detection. A schematic summary of the message format is presented in Figure 2.

Figure 2. Physical Layer Message Format.

The preamble has a sequence of upchirps for the whole frequency band, and sync word is encoded by the last two upchirps. The sync word helps to distinguish among LoRa networks having the same frequency, as end-device configured with specific sync

word, will not give attention to transmission if decoded sync word is different. The preamble length is configurable, and in this study, preamble length $\bar{n} = 8$ symbols. Additionally, 2 bytes of PHDR, 4 bits of PHDR_CRC, the variable length of Payload and 2 bytes of CRC is only present in uplink communication. Equation 3 represents the number of symbols needed to transmit a payload as a function of all given parameters [23]

$$N_{Payload} = 8 + max\left[ceil\left(\frac{8.PL - 4.SF + 16.CRC + 28 - 20.H}{4.(SF - 2.DE)}\right).(CR + 4), 0\right], \quad (3)$$

where *ceil* indicates the ceiling function, SF corresponds to spreading factor values from 7-12, PL is for physical payload length in bytes, CRC represents the presence in the physical frame ($CRC = 1$ when CRC field is present; alternatively it is 0). $H=0$ when the header is enabled, $DE=1$ shows that lower data rate optimization for $SF12$ and $SF11$ and 0 for the remaining SFs while CR is the coding rate.

Receive Window Parameters

The DR for the first receive window ($RX_{1_{DDR}}$) can be defined as the DR for uplink communication lower with DR_{UL} offset RX_{1OFF} (its values range from 0 to 5) [23]. RX_1 will be $DR0$ when RX_{1OFF} is unequal or lower than DR of the uplink. Typically, RX_{1OFF} is zero; therefore, RX_1 has a data rate identical with the DR of previous uplink communication

$$RX_{1_{DDR}} = DR_{UL} - RX_{1OFF}. \quad (4)$$

Similarly, the frequency channel for the RX_1 is same as the prior uplink transmission, whereas RX_2 has the pre-defined frequency and data rate (default frequency 869.525 MHz and data rate $DR0$). These parameters can be configurable depending upon the hardware system. Furthermore, the time needed to sense the downlink preamble properly refers to the duration of the receive window. The radio of end-device remains active for the complete reception of a downlink message. The second receive window (RX_2) will not open if the message has been successfully detected in RX_1. Channel Activity Detection (CAD) mechanism is used to minimize channel listening time for RX_2, as end-device choose sooner to stop preamble detection in case of no incoming signal. Nevertheless, if the message has not been received within RX_1, active components (transceiver and microchip) of device consumes power for a particular time to be in an active mode. This time duration has a direct consequence on the lifetime of an end-device. It is also interesting to note that LoRaWAN protocol does not allow transmission of an uplink before an acknowledgment message for the previous one has been received in either of the receive windows or RX_2 has expired.

2.1.2 LoRaWAN Architecture

LoRaWAN architecture is defined by the following three main components:

- **End-device (ED):** The low-power consumption sensor node that is used to communicate with the gateway to transmit data over the LoRa radio module. EDs usually have embedded energy source to perform distinct processing operations.
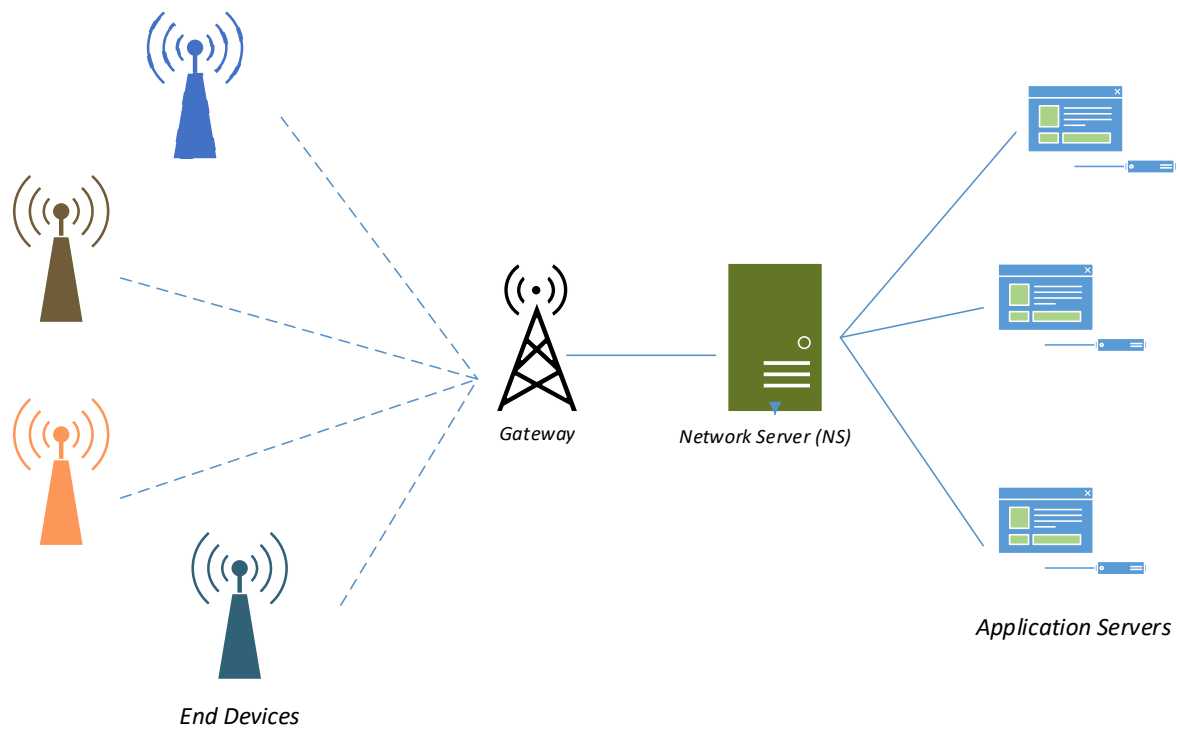
Figure 3. LoRaWAN Network Architecture.

- **Gateway (GW):** It acts as an intermediate entity to forward the data coming from EDs to the network server (NS) and application server (AS), after inserting additional details regarding channel quality. Information is transferred over the IP backhaul network to achieve high throughput [24]. In LoRa deployment, there can be more than one gateway, and the same data can be received (or delivered to NS) by multiple GWs.

- **Network Server (NS):** It acts as a bridge among EDs, GWs, and application servers (AS) in order to guarantee secure and reliable packets routing. NS serves as a brain of the LoRaWAN network for smooth operations execution (de-duplicate and decoding packets, managing acknowledgment slots, and adaptive data rates, etc).

LoRaWAN network is 'a star-of-stars topology' and does not require the EDs to be associated with a specific GW for accessing the network. Logically gateway acts like a link-layer relay; thus, EDs are associated with NS directly. Uplink transmission from node to NS has always encouraged in this bi-directional communication. Figure 3 illustrates the LoRaWAN topology and network architecture. The EDs transmit data messages to GW through the LoRaWAN RF interface. Further, the received data messages are transferred to servers employing IP networks such as 3G/4G, Ethernet, WiFi, etc. Figure 4 demonstrates the protocol stack of LoRaWAN. The ISM bands are defined in the physical layer and LoRa modulation layer is suitable for long range communication with less power consumption. To achieve this, Semtech has implemented the CSS modulation [21].
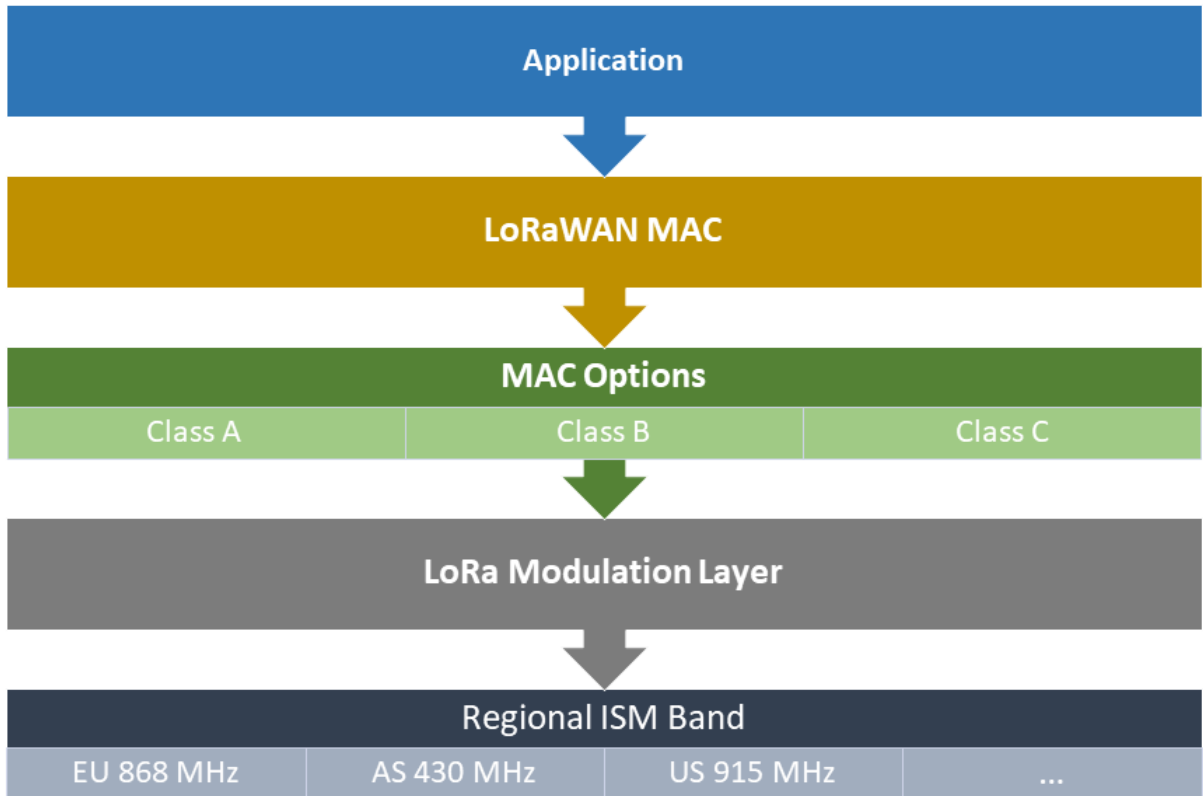
Figure 4. LoRaWAN Protocol Stack.

LoRaWAN specifies three categories of devices (Class A, B, and C) depending upon the application. These classes can coincide in an identical network without providing any definite information to GW [25]. Three classes of EDs are defined by the LoRaWAN imply distinct MAC procedures, which results in to having different power consumption profiles for each class.

Figure 5 illustrates different classes and defined as follow:

1. **Class A:** End-devices use the ALOHA procedure to schedule uplink transmission in bi-directional communication. Class A conducts both uplink and downlink transmission in the same randomly chosen radio channel, which can cause the collision probability. Every node observes the acknowledgment in receive windows (RX_1 and RX_2) during downlink transmission. The delay from termination of an uplink transmission to the start of receive windows (RX_1 and RX_2) is defined as Receive Delay 1 (RX_{1Delay}) and Receive Delay 2 (RX_{2Delay}), respectively. Time offset and data rate are the essential parameters of receiving windows. MAC commands have used to configure time offset or fix at minimum one seconds for RX_{1Delay}. Failure of acknowledgment in RX_1 can only cause the enabling of RX_2. The default values of RX_{1Delay} are 1s and 2s for RX_{2Delay}. Class A devices consume the least power [26].

2. **Class B:** Devices are composed to open extra receiving slots at the scheduled times. A ping slot generated by the gateway to integrate end-devices to receive additional windows. Therefore, a periodic beacon from the gateway for synchronization is

also needed so that the network server (NS) is aware of the listening status of end-devices. Class B devices distribute the radio channel for downlink and uplink transmission to overcome the collision effect. The power consumption of Class B is higher than Class A [25, 27].

3. **Class C:** Nodes consume the most energy since it's characteristic's behavior of continuous listening of channel except during the transmission period [28]. Class C is classified for such IoT applications that have no concerns regarding the power resources.
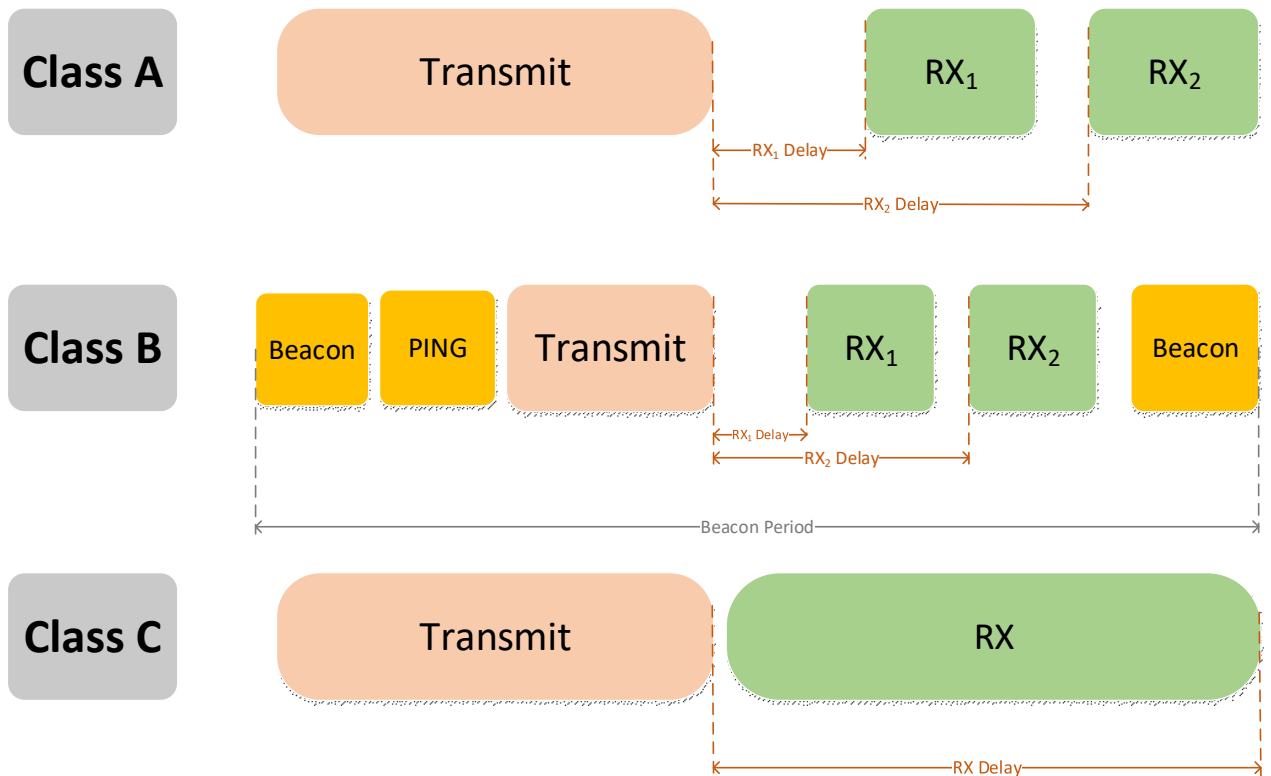
Figure 5. LoRaWAN Classes.

The study provided in this work mainly focuses on Class A end-devices. Casals *et al.* [29] identified 11 different states for Class A LoRaWAN end-device transmission regarding energy consumption:

1. **Wake up:** End-device wake up from sleep state to initiate the transmission procedure.

2. **Radio Preparation:** Radio interface is activated.

3. **Transmission:** The device sends information through the radio interface.

4. **1st Window wait:** Radio mode is deactivated and waits.

5. **1st Receive Window:** Radio has been set up for the receive mode.

6. **2nd Receive Window wait:** If no preamble is received, end-device shut down first receive window and wait.

Table 3. MAC Message Fields

Fields	Length (bytes)
MHDR	1
MIC	4
FHDR	7 - 22
Fport	1
FRM Payload	0 to ($K - 8$)

7. **2nd Receive Window:** Radio is turned on for incoming data, and it must be noted, the shorter time span for the second reception window is of CAD mechanism.

8. **Radio Off:** Radio interface is disabled.

9. **Postprocessing:** Postprocessing on the received information.

10. **Sequence:** End-device disabled all the sequences.

11. **Sleep:** Node goes back to sleep mode.

LoRaWAN does not allow communication between end-devices. Packets can only be transmitted from end-device to gateway or vice versa. LoRa enables adaptive data rate that results in trade-off among throughput for coverage area or energy consumption at a uniform bandwidth.

MAC Message Format

The Physical layer payload comprises of MAC packets. It begins with the Message Header (MHDR) field that provides information regarding the LoRaWAN version and Message Type. There are three distinct message types:

1. Join message.

2. Confirmed Data message.

3. Unconfirmed Data message.

Figure 6 demonstrates the schematic summary of MAC message format. As of the MAC payload, FHDR has detailed information about the end-device short address (DevAddress) and control information in Frame Control field (FCtrl). Fport field is enabled when there is a data in frame payload (FRM Payload), the payload can have MAC commands or application data. Encryption using AES with 128 bits key length is for application data. Message Integrity Check (MIC) entitle a receiver to verify the integrity of MAC received message. Table 3 shows the length of MAC message fields. K represents the maximum length of MAC Payload field.

Table 4. MAC Commands

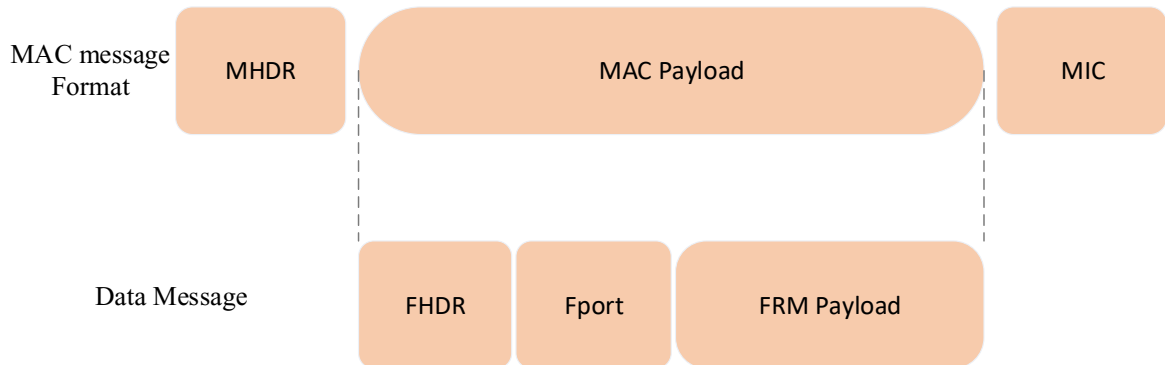| Commands	Description
LinkCheck	Verifying the connection of end-device to the network
DutyCycle	Alter the duty cycle of device for transmission
RXParamSetup	Modify the reception parameters of the node
DevStatus	Allow NS to reset device status
RXTiming	Setup time slots for reception by end-device
TXParam	Amend the transmission parameters

Figure 6. LoRaWAN MAC Message Format.

MAC Command

MAC commands are configured for the modification of communication parameters for LoRaWAN. These commands provide a wide range of customization for radio parameters of end-devices, for instance, empowering NS to have nearly complete control of network status and also optimization of radio channels are presented in Table 4.

Transmission and Retransmission

When a node sends the information in uplink Confirmed transmission, it anticipates receiving the acknowledgment in one of receive windows (RX_1 and RX_2). If the acknowledgment does not acquire in these windows, node transfer the same data until either acknowledgment has been received or the maximum allowed number of MAC layer transmission is achieved. The maximum default number of transmission is 8, and each transmission is performed in different frequency channels depending on the availability of subband channels [30].

It is recommended to follow the next rules for DR selection: 1st and 2nd confirmed message transmission must be performed in the same uplink data rate, 3rd and 4th transmission follow the lower data rate (or $DR0$ if it was lowest data rate) and so on [30]. MAC layer should forward the error code to application layer if message does not receive even after the 8th transmission. Each retransmission begins after the acknowledgment timeout ($ACK_{Timeout}$), a random delay between 1 and 3 seconds [30, 31]. Despite that, duty cycle limit is an additional reason for lack of acknowledgment in return to data

message transmitted by the end-device. Since gateway has required to follow regulations concerning the amount of downlink traffic (comprises acknowledgment to the uplink transmission and also downlink information message from the gateway to nodes). Figure 7 illustrates the acknowledgment structure.
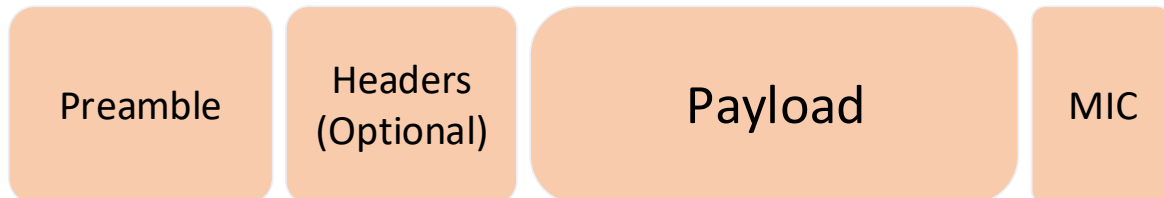

Figure 7. LoRaWAN ACK Structure.

2.2 Related Work

Overviews of LoRa and LPWAN technologies are provided in [22, 32]. Usually, LoRa operates with a bandwidth of 125 kHz, but it also allows for bandwidths of 250 kHz and 500 kHz. The wider bands promote resistance to fading, channel noise, Doppler effects, and long-term relative frequency [32, 33]. Chirp spread spectrum (CSS) modulation, which enables high receiver sensitivity, makes LoRa more robust against interference when compared to SIGFOX, which employs ultra-narrowband (UNB) communication [34]. In Smart Agriculture scenario, where several sensor nodes can be deployed in an agriculture farm over a vast area to transmit measurements i.e., soil pH, temperature, humidity, and water level etc. For instance, LoRaWAN network is deployed at Podere Campáz [35], Forlì FC, Italy, to monitor humidity and soil temperature with two sensor nodes at two locations, merely few meters away from gateway while only employing $SF7$ [36]. Such deployment can be extended to utilize more end-devices employing more spreading factors to cover a large area.

The energy efficiency of sensor network has been investigated in the uncoded system with no Error correction code (ECC) in [37]. Multi-antenna systems utilizing Alamouti diversity schemes have better spectral efficiency as the power consumption of amplifiers and all other circuit blocks comprise average power consumption are considered. In the presence of Rayleigh fading, MIMO system based on said diversity scheme has lower average error probability as compared to SISO because of diversity gain and array gain, which means MIMO consumes less transmission energy as compare to SISO [38]. In addition, Energy efficiency of MISO system apply Alamouti scheme with BPSK modulation in uniform Rayleigh fading during transmission is compared with the reference SISO system.

The work in [39, 40] presents the energy model of low-power sensor node allocated for the wireless network application. A short-range RF module $CC1100$ is used, which does not have the capabilities of LoRa technology. Comparison of LoRaWAN classes and their respective power consumption are reviewed in [41]. The principal objective of this scientific research is to validate the current levels of distinct operating modes issued in LoRa datasheet. Further, the lifetime of end-nodes is estimated based on the measured

results. Despite that, the effect of various LoRaWAN parameters i.e., coding rate (CR), coverage range, and transmission power on total energy consumed are not discussed.

The analytical model of LoRa energy consumption attributed to sleep, transmit, and receive states are proposed [42, 43]. Battery lifetime up to 1 year is achieved with 0.44 mJ energy consumption with optimization of downlink communication in LoRaWAN while considering only a single *SF*. Sensor nodes were transmitting data from 1 to 10 times per hour on two AA batteries in [42]. In [43], a precise calculation for message transmission time in LoRa is introduced. But the study does not give focus on the MAC layer mechanism, in particular message acknowledgment, receive windows (RX_1 and RX_2), and retransmissions.

A single gateway uplink model considering path loss attenuation and Rayleigh fading is designed in [44], utilizing stochastic geometry to model network interference and then disconnection and collision probabilities. Such a model is further extended in [24], in which the authors propose a scheme that considers message replication and gateways with multiple receive antennas/decoders to attain time and spatial diversity. They demonstrate that the number of users and traffic density directly affects the performance of the LoRa network and that sending multiple message copies is beneficial for low-density networks. Both of these studies adopt equal radius *SF* allocation approaches.

Recently several studies presented the power usage and current level of wireless sensor nodes in LoRaWAN networks without proposing an energy model to evaluate and improving energy consumption [45, 46, 47]. Authors in [29] introduced an energy consumption model for LoRaWAN devices. They evaluate the energy consumption of individual devices, disregarding the network behavior. Measurement data are acquired utilizing an existing common LoRa hardware platform, MultiConnect mDot, based on the $SX1272$ transceiver. Unlike [29], our work considers the energy cost and also evaluates the energy efficiency of LoRaWAN networks, considering a network with hundreds of devices.

3 PROPOSED SYSTEM MODEL

In this chapter, we analyze Class-A dense LoRaWAN network consisting of a single gateway relaying messages from $\bar{N}$ uniformly distributed end-devices within a radio range of R km and circular area $V = \pi R^2$. The distribution of sensor nodes is according to the inhomogeneous Poisson point process (PPP) of intensity $p = \bar{N}/V$. Every single point of PPP represents the sensor node. Figure 8 demonstrates a setup with $\bar{N} = 500$ and $R = 3.6$ km. Nodes are distributed uniformly in $V = 40.70$ km^2 around a gateway that is at the origin. It is worth mentioning that such a model exhibits the characteristics of remote sensing applications employed in smart cities, and smart agriculture.
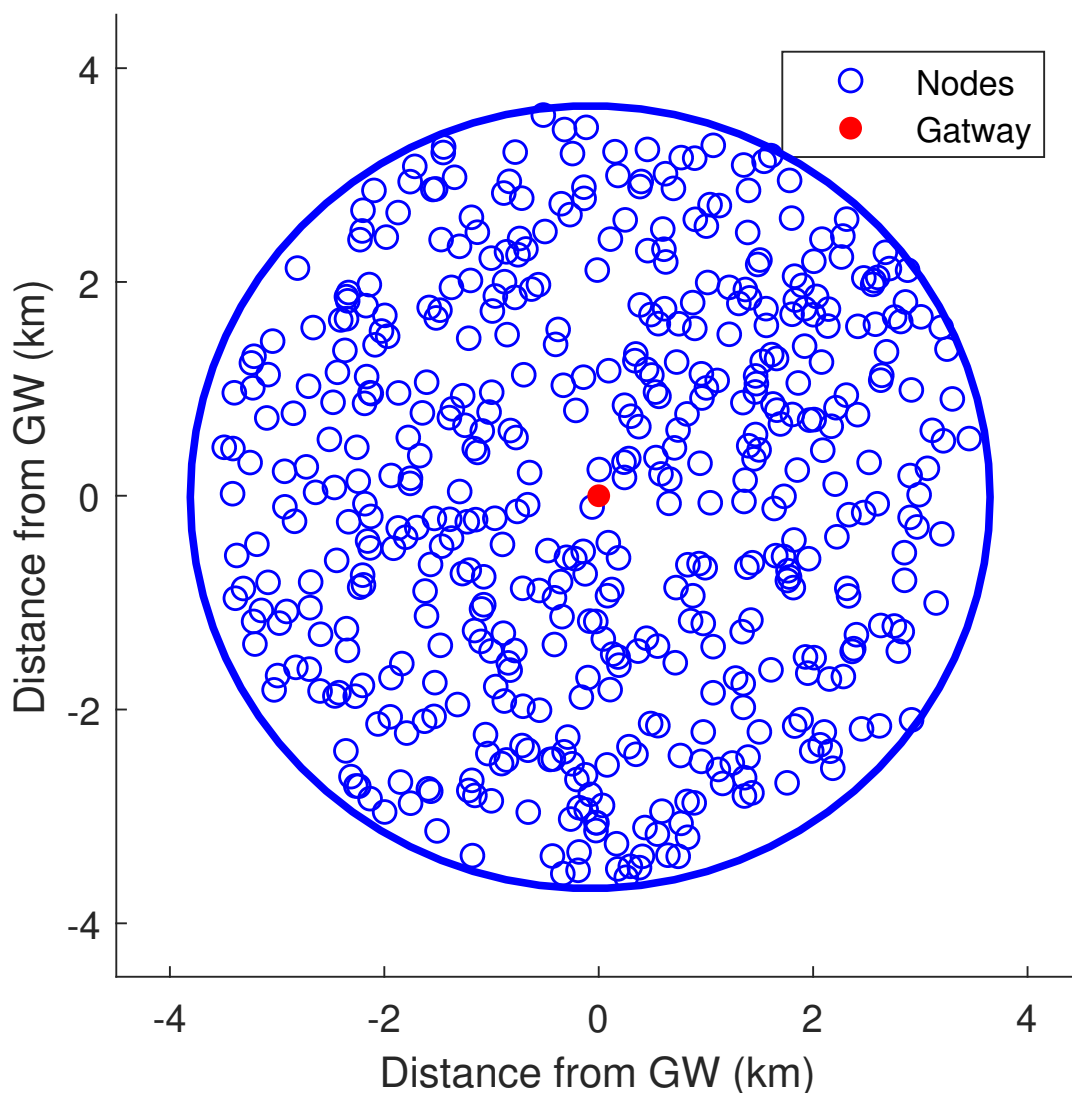

Figure 8. $\bar{N} = 500$ nodes uniformly distributed in a circular network area having radius $R = 3.6$ km.

Different SF allocation strategies are presented in [48], and for simplicity, the spreading factor is assigned on an equal-interval approach on the bases of the system models

Table 5. LoRa uplink model characteristics of 9 byte packets at BW = 125 kHz [24]

DR	SF	Bit Rate Rb_i (kbps)	SNR q_{SF} (dB)	Time-on-Air (ms)	Range (km)
5	7	5.47	-6	41.22	$l_0 - l_1$
4	8	3.13	-9	72.19	$l_1 - l_2$
3	9	1.76	-12	144.38	$l_2 - l_3$
2	10	0.98	-15	247.81	$l_3 - l_4$
1	11	0.54	-17.5	495.62	$l_4 - l_5$
0	12	0.29	-20	991.23	$> l_5$

formulated in [24, 44, 48]. The SF of the devices is allocated according to the distance from the gateway d_i, altered every 600 m, thereby allowing each spreading factor to have the distinct number of end-devices. Thus, sensor nodes in the inner most annulus use the lower SF and the density of each SF increases moving towards the outer annuli, while all the end-devices transmit the data message with the same power, $\mathcal{P}_1 = 14$ dBm.

In our work, we assume $CR = 1$, and the aggregated bit rate of LoRa uplink channel is stated as $bitrate_U = \sum_{i=7}^{12} Rb_i = 12.17$ kbps. As an example, Table 5 summarizes the features of 9 bytes LoRa packets with header and CRC modes enabled at $BW = 125$ kHz [24]. Considering the ToA raises with each SF and the reduction of bit rate in transmitting data message from sensor node to gateway results in increase receiver sensitivity. Therefore maximum coverage area for LoRaWAN is achieved with higher SF.

3.1 Uplink Outage Probability

The uplink transmission of nodes is based on the ALOHA protocol, and the probability of collision in ALOHA networks is high when many stations are connected [49]. In LoRa, simultaneous signals of different SFs are quasi-orthogonal because the inter-SF rejection gain varies from 16 to 36 dB [50]. Therefore, for the sake of simplicity, our work does not inspect inter-SF interference and focuses on co-SF interference only.

In this research work, the uplink model includes the influence of Rayleigh fading and path loss attenuation presented in [33] for performance analysis, where $g\left(d_k\right) = \left(\frac{\lambda}{4\pi d_k}\right)^{\eta}$ is the path loss attenuation function, $\eta \geq 2$ is the path loss exponent, λ is the wavelength, and h_k is the fading in the link between the k-th node and the gateway. Let us consider the transmitted signal of a single LoRa node $s_1\left(t\right)$ to examine the impact of co-SF interference originated due to simultaneous transmission of nodes with same SF. The mathematical expression of the received signal at the gateway can be expressed as

$$r_1\left(t\right) = \sqrt{P\left(t\right)g\left(d_1\right)}h_1 * s_1\left(t\right) + \sum_{k=2}^{N} \chi_k^{SF}\left(t\right)\sqrt{P\left(t\right)g\left(d_1\right)}h_k * s_k\left(t\right) + n\left(t\right), \quad (5)$$

where $n\left(t\right)$ is additive white Gaussian noise with zero mean and variance $\mathcal{N} = -174 + NF + 10\log_{10}(BW)$ dBm, NF is the noise figure of the receiver, -174dBm/Hz is the thermal noise spectral density constant, and BW is the single communicating channel bandwidth.

We consider that an outage of the received signal in an uplink channel can take place in two scenarios [33]. First, if the signal-to-noise ratio (SNR) of the received packet is less than the SF specific threshold q_{SF}, then the node is considered disconnected. Second, if the signal-to-interference ratio (SIR) between the target-received packet and any other concurrent signals of the same SF and frequency channel is less than 6 dB, then it is considered as a collision.

3.1.1 Outage Condition I

The distance of the end-device to the gateway in a wireless transmission domain is crucial. The instantaneous SNR can be expressed as $\text{SNR} = \frac{\mathcal{P}_1 |h_1|^2 g(d_1)}{\mathcal{N}}$, where $\mathcal{P}_1$ is the transmit power of end-device 1 in mW and $|h_1|^2$ is the squared envelop of the channel coefficient. Communication is not possible when the SNR of the received signal at the gateway is less than the reception threshold q_{SF}. Thus, the first outage condition, the connection probability, is defined as [44]

$$H_1 = \exp\left(-\frac{\mathcal{N} q_{SF}}{\mathcal{P}_1 g(d_1)}\right), \tag{6}$$

where d_1 (in meters) is the distance of the desired end-device from the gateway.

3.1.2 Outage Condition II

A collision in LoRa end-device transmission takes place if the SIR of the desired signal with respect to interference from the same SF and frequency channel is less than 6 dB, i.e., if the desired signal is at least four times stronger than the interference. We model this outage condition based on [33], where interference is approached by considering the strongest interfering device. According to [33], the highest interference comes from the end-device k^*.

The probability that no collision occurs or that the strongest interfering signal is at least 6 dB below the desired one, termed the capture probability, is

$$\begin{aligned}
Q_1 &= \mathbb{P}\left[\left.\frac{|h_1|^2 g(d_1)}{|h_{k^*}|^2 g(d_{k^*})} \geq 4 \,\right|\, d_1\right] \\
&= \mathbb{E}_{|h_1|^2}\left[\mathbb{P}\left[\left. X_{k^*} \leq \frac{|h_1|^2 g(d_1)}{4} \,\right|\, |h_1|^2, d_1\right]\right].
\end{aligned} \tag{7}$$

The probability above depends on the distribution of $X_{k^*} = |h_{k^*}|^2 g(d_{k^*})$. The cumulative distribution function (CDF) of X_{k^*} is derived in [44] and is denoted as $F_{X_{k^*}}$. Thus,

$$\begin{aligned}
Q_1 &= \mathbb{E}_{|h_1|^2}\left[F_{X_{k^*}}\left(\frac{|h_1|^2 g(d_1)}{4}\right)\right] \\
&= \int_0^\infty e^{-z} F_{X_{k^*}}\left(\frac{z g(d_1)}{4}\right) \, \mathrm{d}z.
\end{aligned} \tag{8}$$

Moreover, in [44] the authors present an approximation for (8) that is only accurate at the edges of each annulus. This work considers only the exact probability in (8).

3.1.3 Coverage Probability

The probability that defines whether a selected end-device is in coverage and can successfully communicate with the gateway is termed the coverage probability. It is the product of H_1 and Q_1 which means that the node has to be connected and not collided. The average coverage probability $\wp_c$ can be achieved by deconditioning the location of the individual node by averaging over the network coverage area $V = \pi R^2$, i.e.,[44]

$$\wp_c = \frac{2}{R^2} \int_0^R H_1(d_1) Q_1(d_1) d_1 \ dd_1. \tag{9}$$

The average coverage probability of a individual SF annulus is also inspected. It indicates the probability of an end-device at distance d_1 in the annulus i by considering the connection and capture probabilities and is defined as [24]

$$\wp_{c,i} = \frac{2}{(l_{i+1} - l_i)^2} \int_{l_i}^{l_{i+1}} H_1(d_1) Q_1(d_1)(d_1 - l_i) \ dd_1, \tag{10}$$

where l_{i+1} is the radius of the outer circle and l_i is the radius of the inner circle of the ith annulus.

The outage probability translates as the selected node is unable to successfully communicate with the gateway in regard to connection and collision outage conditions. The average outage probability of LoRaWAN network is dependent on the average coverage probability and can evaluate as

$$\wp_{outage} = 1 - \wp_c. \tag{11}$$

This chapter is further divided into two sections to define the models for the communication of data in unconfirmed and confirmed transmission, i.e., unacknowledged and acknowledged transmission for all SFs.

3.2 Power Consumption of Unacknowledged Transmission

Following [29], consider $\bar{N}$ nodes of characteristics of MultiConnect mDot platform [23] on the bases of $SX1272$ transceivers [51]. For LoRaWAN transmission, mDot platform provides a decrease in low current consumption when voltage reduces from 5 V to 3.3 V, which is the minimum operating voltage of the device. For unacknowledged transmission, power consumption is irrespective of Bit error rate (BER) since end-device will dissipate the same energy for every transmission, and also there is no retransmission for unacknowledged communication.

Time and current consumption measurements of a single node defining all its states are summarized in Table 6. The time during two sequential message transmission by node is notification period T_{Notf}. Current consumption for average unacknowledged transmission $\bar{I}_{unAck}$ is [29]

$$\bar{I}_{unAck} = \frac{1}{T_{Notf}} \sum_{i=1}^{N_{states}} T_i.I_i, \tag{12}$$

Table 6. Time and Current Consumption for LoRaWAN unacknowledged transmission [29]

State Number	Time		Current	
	Symbol	Value(ms)	Symbol	Value(mA)
1	T_w	168.2	I_w	22.1
2	T_{rp}	83.8	I_{rp}	13.3
3	T_{tx}	see Table 7	I_{tx}	83
4	T_{1w}	983.3	I_{1w}	27
5	T_{RX_1}	see Table 7	I_{RX_1}	38.1
6	T_{2w}	Equation (15)	I_{2w}	27.1
7	T_{RX_2}	33	I_{RX_2}	35
8	T_{ro}	147.4	I_{ro}	13.2
9	T_{pp}	268	I_{pp}	21
10	T_{seq}	38.6	I_{seq}	13.3
11	T_{sl}	Equation (13)	I_{sl}	45×10^{-3}

where T_i, I_i refers to duration and current consumption of state i. The duration of sleep state can evaluate with respect to notification time and active transmission states i.e. all states except the sleep state is defined as [29]

$$T_{sl} = T_{Notf} - T_{active} \,, \tag{13}$$

where T_{active} indicates the sum of all transmission states except sleep states [29]

$$T_{active} = T_w + T_{rp} + T_{tx} + T_{1w} + T_{RX_1} + T_{2w} + T_{RX_2} + T_{ro} + T_{pp} + T_{seq} \,, \tag{14}$$

as T_{2w} rely on the the receiver window delays and also on T_{RX_1}. The default values of RX_{1Delay} is 1 second, and 2 seconds for RX_{2Delay}. Thus duration of second receive window can be evaluated as [29]

$$T_{2w} = RX_{2Delay} - RX_{1Delay} - T_{RX_1} \,, \tag{15}$$

$$T_{RX_1} = N_S * T_S \,, \tag{16}$$

where N_S indicates the number of symbols for which end-device remains in receive mode. For $SF12$ and $SF11$, N_S is 8 symbols and 12 symbols for remaining SFs.

T_{tx} corresponds to time duration needed for an end-device to transmit preamble and physical message through radio interface while considering LoRaWAN procedures, modulation and regional regulations [51]

$$T_{tx} = T_{pre} + T_{PHY} \,, \tag{17}$$

From [52], we have

$$T_{pre} = (4.25 + N_{pre}).T_S \,, \tag{18}$$

where N_{pre} is the number of programmable preamble symbol utilized by radio transceiver. The physical message duration can be determine as [51]

$$T_{PHY} = T_S * N_{Payload} \,. \tag{19}$$

Table 7. Values of Relevant Parameters used for LoRaWAN transmission [29]

SF	T_S (ms)	T_{pre} (ms)	T_{RX_1} (ms)	T_{RX_2} (ms)	Max FRM Payload (bytes)	T_{tx} (ms)	
						Uplink	Downlink
12	32.77	401.41	262.14	33.02	51	2793.5	991.8
11	16.38	200.70	131.07	16.64	51	1560.6	577.5
10	8.19	100.35	98.30	8.45	51	698.4	288.7
9	4.10	50.18	49.15	4.35	115	676.9	144.4
8	2.05	25.09	24.58	2.30	242	707.1	72.2
7	1.02	12.54	12.29	1.28	242	399.6	41.2

Table 7 outlines the basic parameter with their main values used in our system model. Receiver will be in the active mode for second receive window (RX_2) during a small proportion of CAD state (Section 2.1.1). This proportion is T_{RX_2}, that can evaluate as [29]

$$T_{RX_2} = \frac{2^{SF} + 32}{BW} . \tag{20}$$

After modeling T_{tx} and other relevant required variables to evaluate $\bar{I}_{unAck}$, the average power consumption of an end-device in transmitting data message to the gateway are measured by the Equation 21

$$\bar{P}_{unAck} = V.\bar{I}_{unAck} , \tag{21}$$

where V represents the battery voltage of 3.6 V. The lifetime of the node operated for unacknowledged transmission can be obtained as a function of battery capacity C_B (2400 mAh) [29]

$$T_{lt-unAck} = \frac{C_B}{\bar{I}_{unAck}} , \tag{22}$$

considering the linear behaviour of a battery in ideal scenarios. However in real-life scenario, battery characteristics degrades over the time. Hence, these findings will only provide the approximation on the real node lifetime.

Further, an equally important performance parameter to be considered is the energy cost of data transmitted in unacknowledged mode. It contributes to provide information about the energy required by the end-device per each delivered bit of data payload, as in [29]

$$EC_{del-unAck} = \frac{\bar{P}_{unAck}.T_{Notf}}{l_{payload}} , \tag{23}$$

where $l_{payload}$ indicates the FRM Payload field size (Table 7).

3.3 Power Consumption of Acknowledged Transmission

In this section, the model for an average power consumption $\bar{P}_{Ack}$ of a sensor node in the acknowledged transmission mode is defined, when the BER is zero. Acknowledgment can be transmitted in the first receive window RX_1 or second receive window RX_2. In this research work, we considered both approaches.

Casals *et al.* [29] defined the current consumption profile of a sensor node in two distinct approximations which are considered to evaluate the average power consumption of acknowledged transmission:

1. For $SF7$ and $SF8$, average power consumption $\bar{P}_{Ack_1}$ is calculated considering acknowledgments obtained in first received window (RX_1).

2. For $SF9$–$SF12$, Acknowledgments acquired in the second received window (RX_2) to constitute average power consumption $\bar{P}_{Ack_2}$.

The FRM Payload size for every SF can be obtained from Table 7. When the acknowledgment is received in first receive window, then the states involved in this approach reduces as compared to unacknowledged transmission, given that end-device does not have to open second receive window. However, the time duration for first receive window and radio off interval increases, considering acknowledgment to be properly acquired and afterward processed. Therefore, $\bar{P}_{Ack_1}$ is evaluated likewise $\bar{P}_{unAck}$ for the same operating SF except setting T_{2w} and T_{RX_2} to 0 in Equation 14. Table 8 outlines the principle states for acknowledged transmission and their respective values.

Table 8. Time and Current Consumption for LoRaWAN Acknowledged transmission, when acknowledgment is acquired in first receive window [29]

State	Time		Current	
Number	Symbol	Value(ms)	Symbol	Value(mA)
1	T_w	169.2	I_w	22.1
2	T_{rp}	80.4	I_{rp}	13.7
3	T_{tx}	see Table 7	I_{tx}	82.8
4	T_{1w}	988.4	I_{1w}	27.1
5	T_{RX_1}	T_{tx} *Downlink* in Table 7	I_{RX_1}	31.8
8	T_{ro}	337.8	I_{ro}	13.4
9	T_{pp}	272.5	I_{pp}	20.9
10	T_{seq}	37.5	I_{seq}	13.4
11	T_{sl}	Equation (13)	I_{sl}	45×10^{-3}

Similarly $\bar{P}_{Ack_2}$ is computed, the only difference with $\bar{P}_{unAck}$ is the increase in duration of second receive window (T_{RX_2}) and successive radio off interval (T_{ro}) in $\bar{P}_{Ack_2}$. Actually, an end-device is required to remain in the receive window to entirely acquire the acknowledgment from the gateway. Consequently, $\bar{P}_{Ack_2}$ can evaluate through the same equations as for $\bar{I}_{unAck}$. From [29], the numerical values of second receive window duration plus radio off is highlighted in Table 9.

Table 9. Time and Current Consumption for LoRaWAN Acknowledged transmission, when acknowledgment is acquired in second receive window [29]

State	Time		Current	
Number	Symbol	Value(ms)	Symbol	Value(mA)
7	T_{RX_2}	T_{tx} *Downlink* in Table 7	I_{RX_2}	38
8	T_{ro}	337.8	I_{ro}	13.4

Average power consumption of the sensor node in sending information message to the gateway in confirmed transmission mode is

$$\bar{P}_{Ack} = V.\bar{I}_{Ack} \,. \tag{24}$$

Theoretical lifetime of an end-device performing operation on battery in acknowledged transmission mode, represented T_{lt-Ack}, based on the battery capacity C_B and average current consumption $\bar{I}_{Ack}$ is expressed next [29]

$$T_{lt-Ack} = \frac{C_B}{\bar{I}_{Ack}} \,. \tag{25}$$

The energy cost $EC_{del-Ack}$ of an end-device in delivering the data message during acknowledge transmission is provided, as in [29]

$$EC_{del-Ack} = \frac{\bar{P}_{Ack}.T_{Notf}}{l_{payload}} \,. \tag{26}$$

3.4 Average Energy Cost and Energy Efficiency

Since we assume the effect of Rayleigh fading on the average power consumption of nodes communicating in LoRaWAN network, thus average energy cost $\wp_{EC}$, can be achieved similar to (9)

$$\wp_{EC} = \frac{2}{R^2} \int_0^R \frac{EC_x(d_1)}{H_1 Q_1(d_1)} d_1 \; \mathrm{d}d_1 \,, \tag{27}$$

where $EC_x = \{EC_{del-unAck}, \; EC_{del-Ack}\}$ and d_1 is the Euclidean distance of end-device from the gateway.

The consumed energy relates to a total amount of transmit power while delivering data payload among nodes and gateway. The energy cost of sensor node per delivered bit is evaluated as

$$EC_{bit-i} = \frac{EC_i}{LS(\bar{N}, M).l_{data_i}} \,, \tag{28}$$

where i and l_{data} indicate the $SF = \{7,8,9,10,11,12\}$ and complete size of data message also comprising all headers corresponding to each spreading factor, respectively. Furthermore, a successful transmission link is identified as Link Success LS, which is a function of an average number of nodes $\bar{N}$ and number of message replication M. In this context, coverage probability per SF ($H_1 Q_{1_i}$) is referred as link success

$$LS_i(\bar{N}, M) = H_1 Q_{1_i} \,. \tag{29}$$

Energy Efficiency is defined by reducing energy consumption while performing the same tasks and operations. Since it is not practical to replace or recharge batteries of end-devices, thus optimizing energy usage is of utmost importance and essential in the LoRaWAN network. Additionally, the number of nodes present in each spreading factor N_i assist for Energy Efficiency, which can be determined from

$$EE_{bit-i} = \frac{EC_{bit-i}}{N_i} \,. \tag{30}$$

Energy Efficiency of LoRaWAN network is highly dependent on an average number of nodes $\bar{N}$ and outage probability encountered by them while concurrently transmitting data messages in confirmed or unconfirmed transmission mode. Since connection probability H_1 only relies on the distance between an end-device and the gateway, which makes capture probability Q_1 mostly responsible for the deterioration of the transmission network. That happens as Q_1 is affected by the increase in medium usage, which, in turn, increases network interference. Furthermore, ToA with each SF substantially grows causes Q_1 to decreases after every 600 m. The energy efficiency of LoRaWAN is a function of the feasible number of nodes in a specific SF

$$
\begin{aligned}
N^* &= \arg\max_{N_i} EE_{bit-i} \\
&= \arg\max_{N_i} \frac{EC_i}{LS(\bar{N}, M).l_{data_i}} \frac{1}{N_i} \, .
\end{aligned}
\tag{31}
$$

It is essential to highlight that the analytical solution of Equation 31 is not achievable, since dependency of adequate transmission of information message on coverage probability $H_1 Q_1$. Moreover, it is not possible to find a derivative of capture probability Q_1.

4 NUMERICAL RESULTS AND EVALUATION

In this chapter, we evaluate the system model derived in Chapter 3 for assessing the power consumption, lifetime, and energy cost of data message delivered by the end-device in the LoRaWAN network. Additionally in Section 4.5, the energy cost of the network is computed as a function of each SF for distinct notification time (i.e. $T_{Notf} = \{1, 5, 20, 50, 100\}$ min) .

The chapter is subdivided into six sections, each emphasis on the performance parameter of the LoRaWAN network. Table 10 summarizes the parameters considered for the evaluation purposes

<div align="center">Table 10. System Parameters</div>

Parameter	Symbol	Value
Nodes	$\bar{N}$	500
Network Radius	R	3.6 km
Transmit Power	$\mathcal{P}_1$	14 dBm
Spreading Factor	SF	7–12
Width of SF Annulus	R_{l_i}	600 m
Bandwidth	BW	125 kHz
Carrier frequency	f	868 MHz
Noise figure	NF	6 dBm
Duty cycle	p_0	1%
Path loss exponent	η	2.75

4.1 Average Power Consumption of Unacknowledged Transmission

We have assessed the average power consumption of a single end-device transmitting data message to the gateway by exploiting numerical values from Tables 6 and 7 and Equations (1), (3), (12)-(21). Unacknowledged communication is unrelated concerning BER, since node performs a single transmission attempt, despite the fact whether it is properly received by network server or not.

Figure 9 demonstrates the average power consumption $\bar{P}_{unAck}$ as a function of increasing notification time T_{Notf} for each SF. The 1% duty cycle limitation provides the minimum notification time and this constraint is also applicable to sub-bands channels and SF. The average power consumption predictably decreases with the increase of notification time, given that the sleep state is mostly dominant entity while other states remain to have minimum active duration. Thus, $\bar{P}_{unAck}$ inclines towards sleep current while T_{Notf} grows larger.

On the contrary, SFs have a proportional relationship with average power consumption as transmit and receive intervals of sensor nodes are inversely correlated with each spreading factor. Further, the time-on-air (ToA) increases with decreasing bit rate for each SF. Nevertheless, the difference among average power consumption for each SF reduces as T_{Notf} raises.
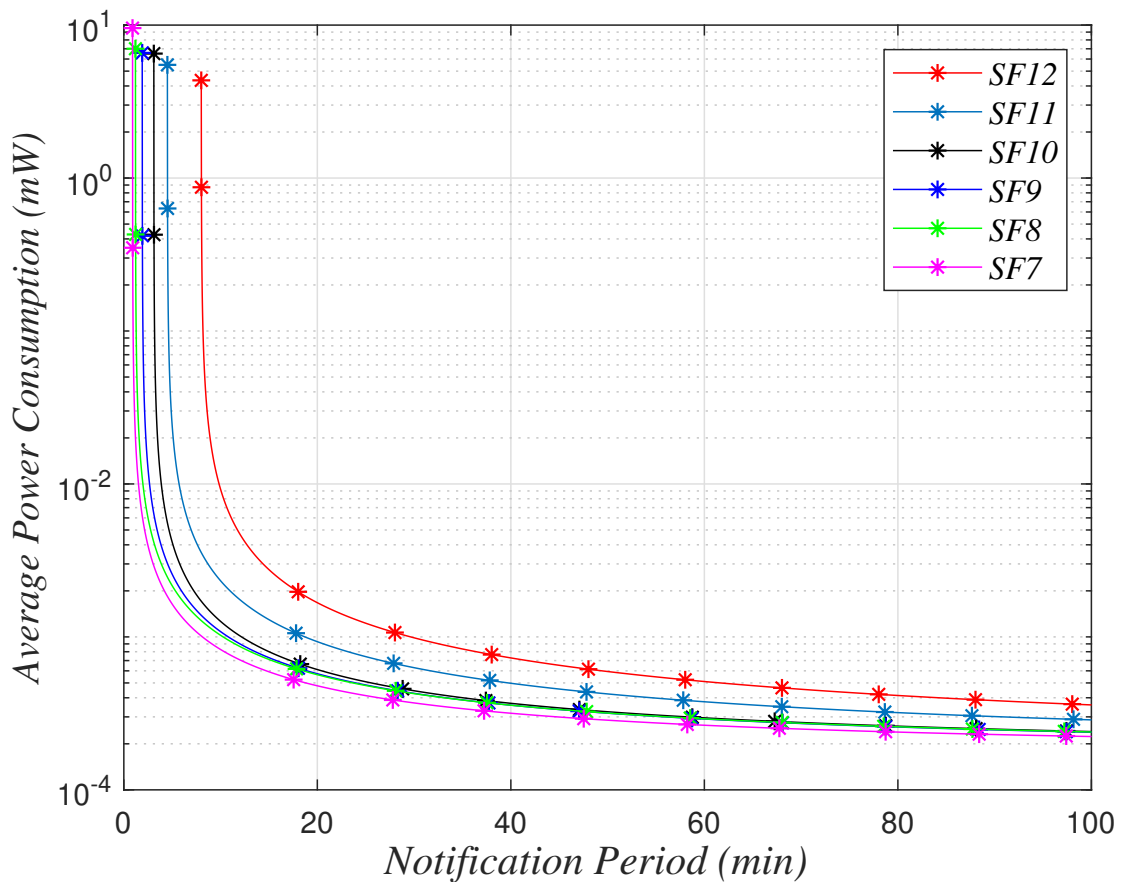
Figure 9. $\bar{P}_{unAck}$ of a single node as a function of T_{Notf} for each SF.

4.2 Average Power Consumption of Acknowledged Transmission

We evaluate the average power consumption of a single end-device in an acknowledged transmission through values from Table 7–9. Figure 10 illustrates the characteristics of end-device performing acknowledged transmission for different notification time duration. The tendency of average power consumption toward sleep current is similar in acknowledged transmission as it was in unacknowledged transmission. Furthermore, $\bar{P}_{Ack}$ reduces with the increase in T_{Notf}, and also altering to higher SF.
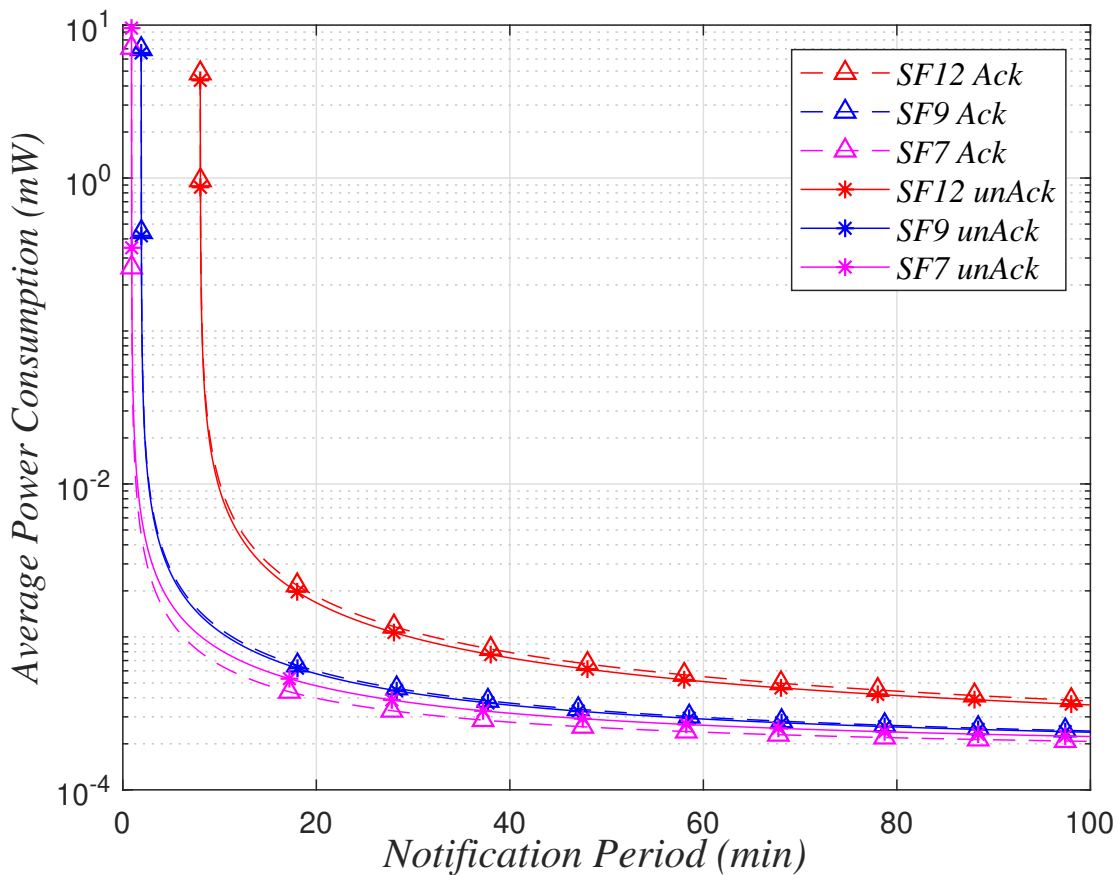
Figure 10. Comparison of $\bar{P}_{unAck}$ and $\bar{P}_{Ack}$ of a single end-device in terms of T_{Notf} for different SFs.

It is interesting to have a notable observation about the characteristic performance of acknowledged link layer protocol is that it depletes less power in comparison with the unacknowledged transmission. Since the acknowledgment message can be received by the sensor node in the first receive window or second receive window. The last-mentioned will constitute to higher power consumption for $SF = \{9, 10, 11, 12\}$ for confirmed transmission, as acknowledgment has to be acquired appropriately, which turns into larger T_{RX_2} and T_{2w}. Although the former leads to lower power consumption, since then, the end-device does not have to worry about the second receive window and its waiting time (Section 3.3).

4.3 Average Outage

We next evaluate the average outage as the function of an average number of nodes for different duty-cycles $p_0 = \{0.1, 0.5, 1\}\%$. From Equation (11) and Figure 11, it is evident that the average number of nodes have a proportional relation with the average outage in LoRaWAN network.

The highly dense network will contribute to excessive collision probability and has a direct impact of the co-spreading factor, where it is less probable for the requested signal
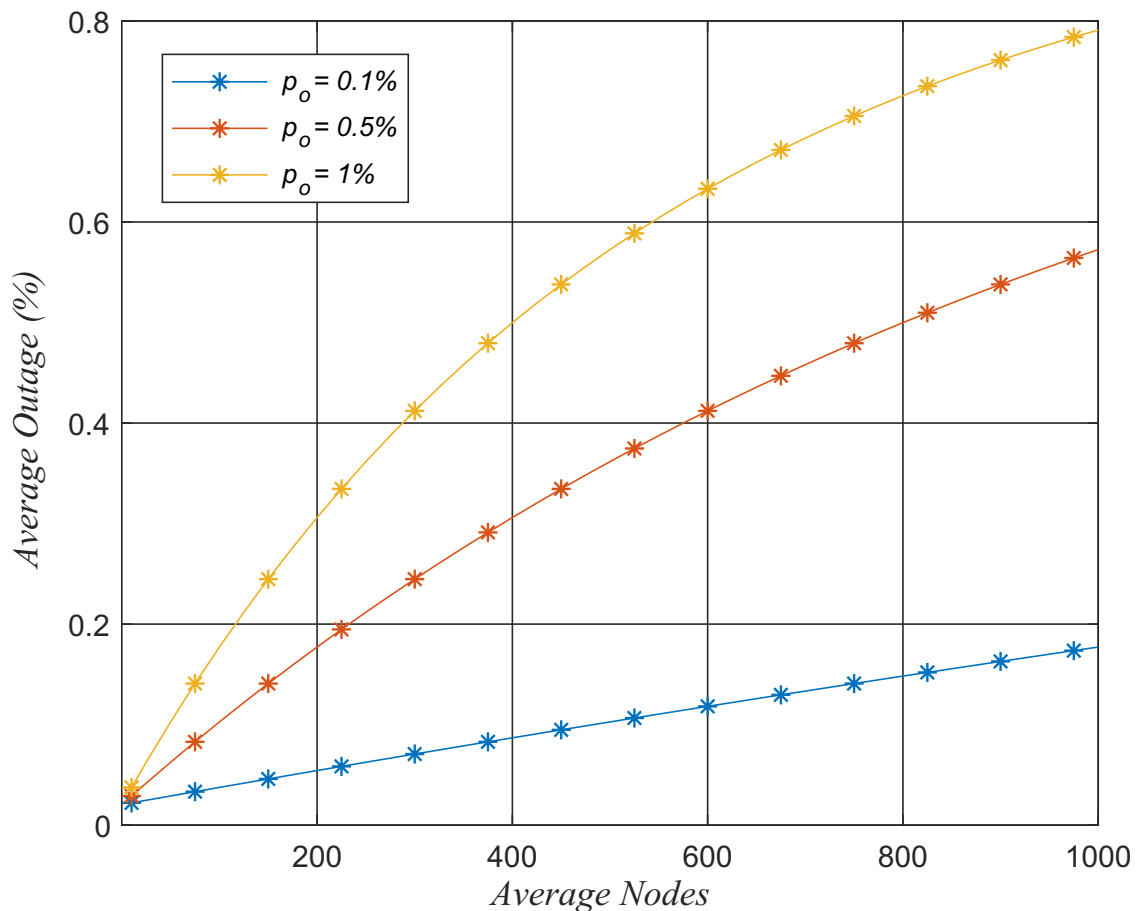
Figure 11. Average outage probability $\wp_{outage}$ as function of average number of nodes $\bar{N}$ for different duty cycles p_0

to be four times stronger than the interfering signal of an identical frequency channel and spreading factor. Therefore, for the end-device, it is challenging to communicate properly to the gateway. Capture probability Q_1 degrades with each SF since outer annuli are bigger in area as compared to inner annuli. It is due to the uniform distribution of sensor nodes in the circular coverage region. Thus, this distribution provides a higher spreading factor to facilitate more nodes than lower SFs. As a result, the network encounter co-SF interference that deteriorates the overall transmission performance.

4.4 Lifetime of End-device

The theoretical lifetime of an end-device is computed employing average power consumption results acquired in 4.1 and 4.2 for unacknowledged transmission and acknowledged transmission by using Equations (22) and (25).

Figure 12 demonstrates the lifetime of end-device in unacknowledged transmission in terms of notification time T_{Notf} for each SF, assuming zero BER. The capacity of battery in our work is assumed of 2400 mAh. Node will have a better lifetime value

when it transmits one message periodically for a higher notification period. Table 11 summarizes the different lifetime can be achieved based on the distinct notification time for unacknowledged transmission. The maximum lifetime value of 4.4 years can be achieved with exploiting features of $SF7$ and a notification period of 100 min. Transmission of a data message through higher SF has an adverse effect on a lifetime of the sensor node due to most power consumption.

Table 11. End-device lifetime for LoRaWAN Unacknowledged transmission

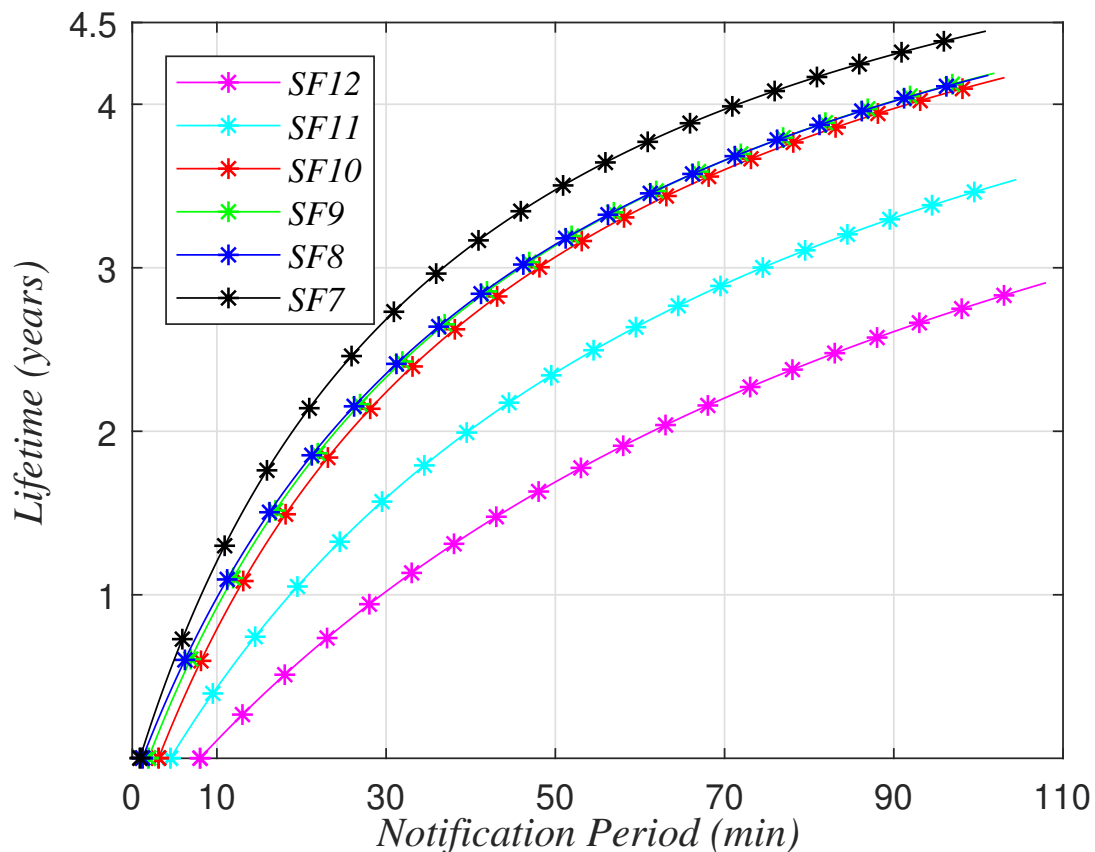| T_{Notf} (min)	End-device Lifetime (years)					
	$SF7$	$SF8$	$SF9$	$SF10$	$SF11$	$SF12$
10	1.2	1	0.93	0.78	0.43	0.11
20	2.07	1.78	1.74	1.62	1.08	0.60
50	3.47	3.15	3.14	3.06	2.35	1.69
100	4.4	4.17	4.16	4.12	3.46	2.78

Figure 12. Sensor Node lifetime in unacknowledged transmission $T_{lt-unAck}$ as a function of T_{Notf} for different SFs.

Similarly, the lifetime upper bound of sensor node for acknowledged transmission is demonstrated in Figure 13. Since, average power consumption of end-device is in inverse relation with the lifetime, therefore lower power consumption will produce the

greater operational lifetime. Table 12 outlines the lifetime of end-device for acknowledged transmission.

Table 12. End-device lifetime for LoRaWAN Acknowledged transmission

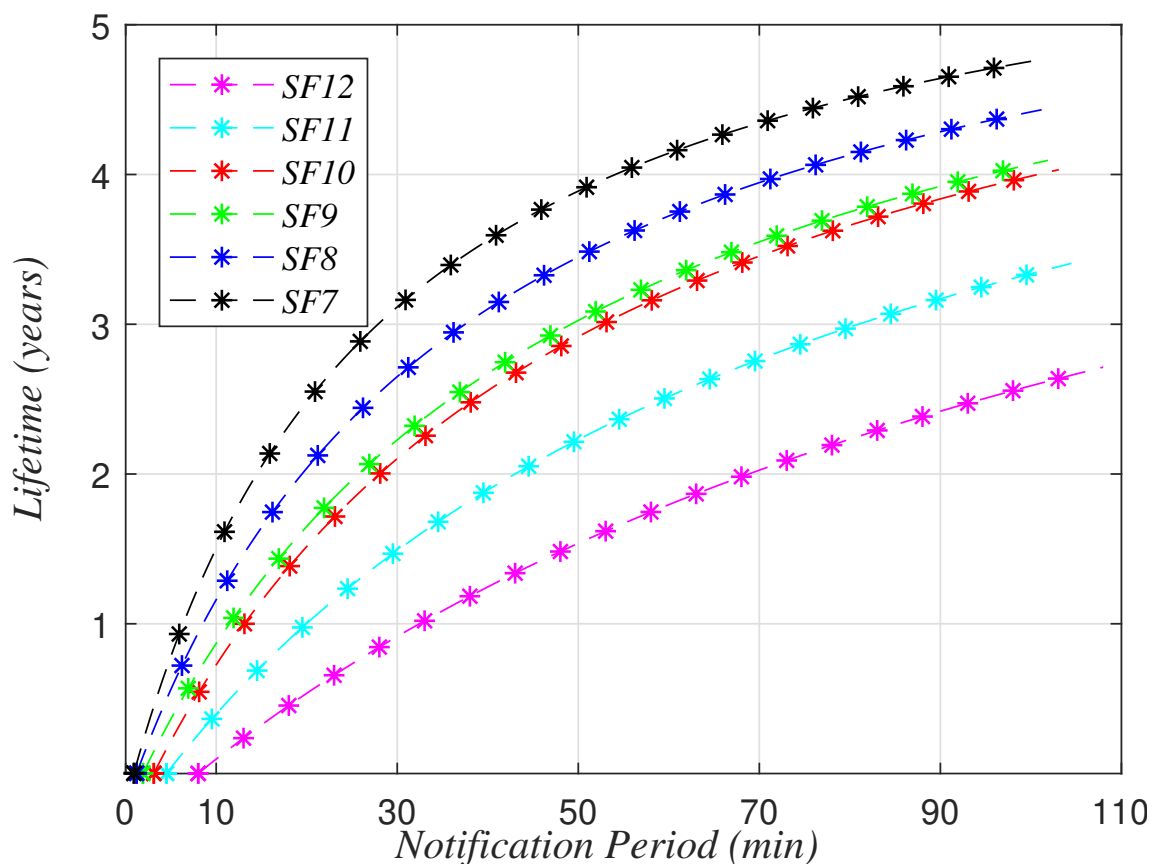| T_{Notf} (min)	End-device Lifetime (years)					
	$SF7$	$SF8$	$SF9$	$SF10$	$SF11$	$SF12$
10	1.5	1.12	0.86	0.72	0.4	0.09
20	2.49	2.01	1.16	1.15	1	0.5
50	3.88	3.45	3.03	2.92	2.23	1.54
100	4.76	4.41	4	3.99	3.34	2.59

Figure 13. Sensor node lifetime in acknowledged transmission T_{lt-Ack} in terms of T_{Notf} for distinct SFs.

It is observed from Tables 11 and 12, that the maximum value of a lifetime is achieved in acknowledged transmission with exploiting lower spreading factors (i.e., $SF7$ and $SF8$) compared with unacknowledged transmission having similar parameters. Since power consumption is minimum due to the opening of only one receive window (RX_1). In contrast, for higher spreading factor, the opening of both receive window and their respective waiting time results in higher average power consumption, which makes up less lifetime of end-device in acknowledged transmission.

4.5 Energy Cost

In this subsection, one of the main performance parameters, i.e., the energy cost of transmitting data messages from an end-device to the gateway for unconfirmed mode is evaluated. From Equation (23) to compute $EC_{del-unAck}$, we move the node location from the inner annuli to the outermost annuli with a fixed step size. These findings help to determine the average energy cost of LoRaWAN network through (27). 2400 mAh battery capacity with 3.6 V voltage is assumed in this work.

The distance of the end-device from the gateway has considerable influence on connection probability. However, H_1 is not dependent on the duty cycle or the average number of sensor nodes. Moving towards the capture probability Q_1, unlike H_1, it considers the co-SF interference. Q_1 declines gradually with increasing SF, this trend is because of two significant factors including ToA and the number of nodes in each annulus [33]. ToA grows exponentially with SF; thus, for the higher SFs, the wireless channel remains occupied for a long time slot, which increases the risk of collisions between simultaneously transmitted LoRa packets. In the same way, the number of end-devices in an individual annulus increases for higher SFs due to the uniform distribution of nodes in the circular coverage area. As a result, the network experiences co-SF interference that degrades the quality of transmission.
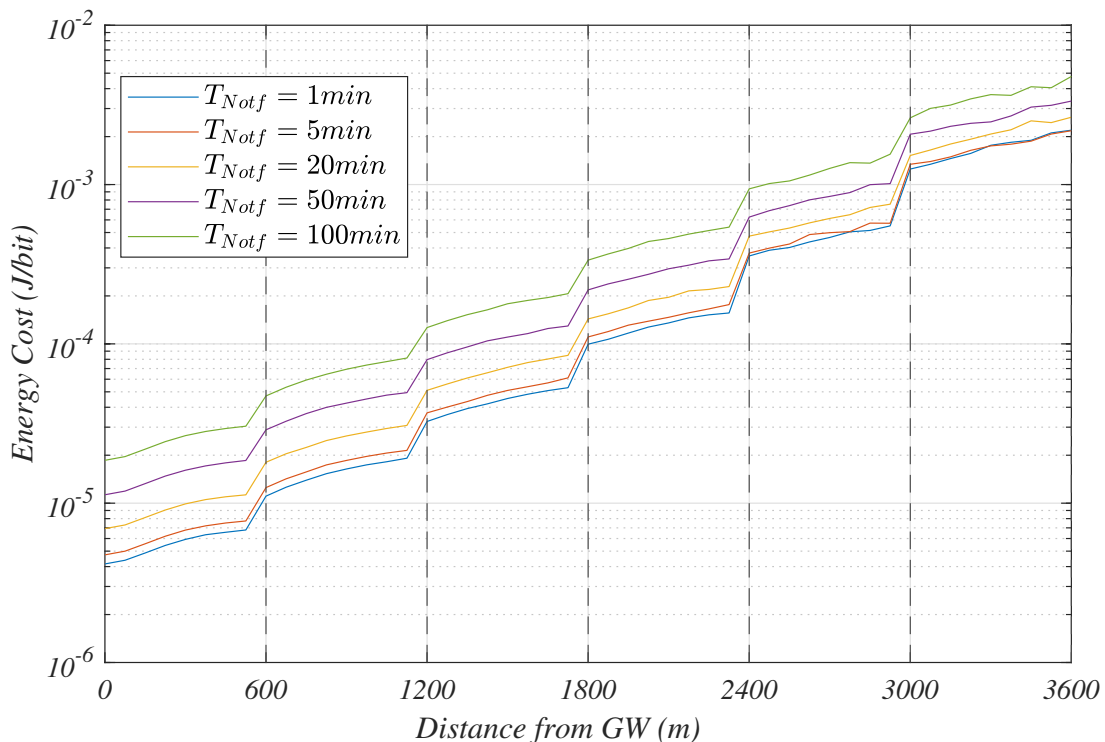

Figure 14. Energy cost $EC_{del-unAck}$ of end-device in unacknowledged transmission as varying distance from gateway GW.

Figure 14 illustrates the average energy cost $\wp_{EC}$ for the unacknowledged transmission scenario at the varying $T_{Notf} = \{1, 5, 20, 50, 100\}$ min, and an average number of nodes $\bar{N} = 500$. The FRM Payload size is 30 byte for all SFs. The spreading factor changes

with every 600 m distance of end-device from gateway. Our study evaluated the average energy cost considering the analytical model, realistic parameters, and averaging over 10^4 random deployment of the Poisson point process (PPP) by Monte Carlo computer simulations.

Nodes that employ characteristics of lower SF consumes the minimum energy cost since the data message is transmitted with a high data rate and less ToA. Such effect is observed in $SF = 7, 8$, and 9 until it tends to increase for the remaining spreading factors. End-devices that operate with $SF12$ deplete the majority of energy, considering data message will be delivered with higher time-on-air and lowest data rate. Since the wireless channel remains occupied for a longer time in higher SFs due to larger ToA, which increases the risk of collision among concurrently transmitted data messages. The energy consumption of the sensor node increases with the growth of notification time. $SF12$ shows higher energy cost as compared to $SF11$ because of a lower bit rate for $SF12$, which, in turn, result in larger transmit time and also receive window duration. Furthermore, the energy cost raises with an increase of T_{Notf}. Therefore, the notification time of 100 min at higher SF will cause more energy cost.

We also study the impact of the average number of nodes on the average energy consumption of the LoRaWAN network (Figure 15) for $T_{Notf} = 5$ min. The energy cost highly depends on the medium usage, which contributes to coverage probability, since dense network promote collision among the concurrently communicating end-devices which leads to increase the energy required to adequately transmit data message.
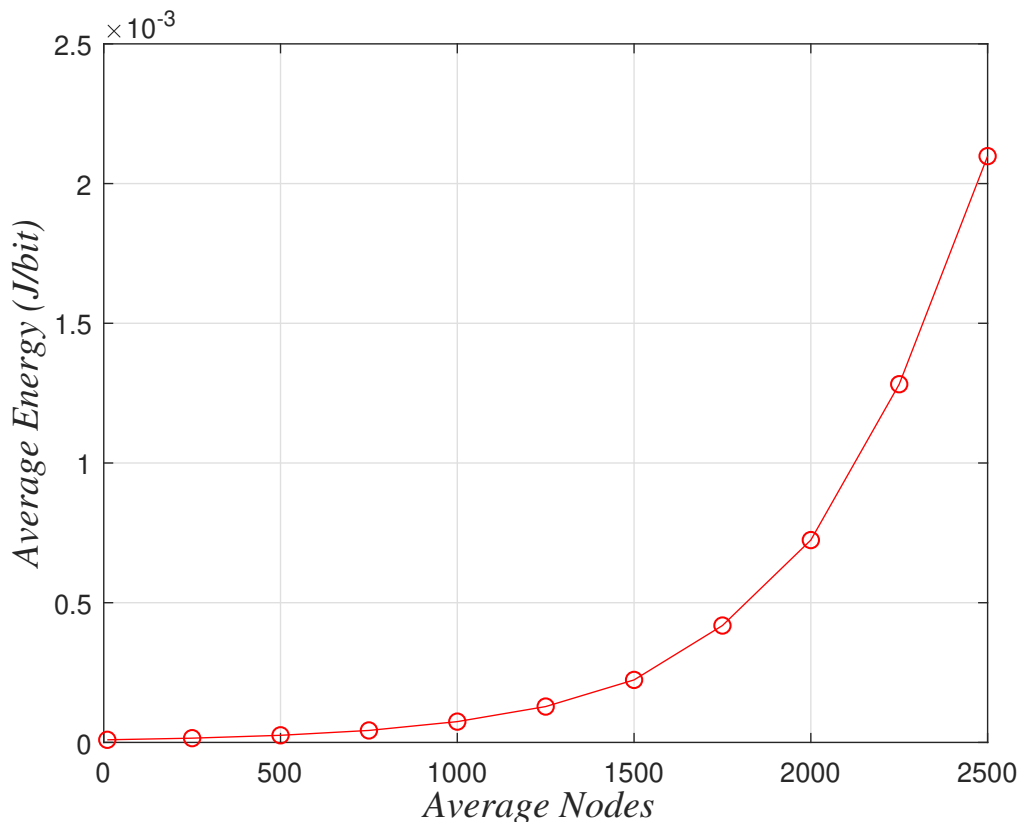

Figure 15. Impact of Average number of nodes $\bar{N}$ on the average energy consumption of LoRaWAN Network.

4.6 Energy Efficiency

In this subsection, we compute the energy efficiency of end-devices in unacknowledged transmission mode, based on the analytical method defined in Section 3.4 and on (28) to (30). Figure 16 illustrates the characteristic's behavior of each SF with a distinct number of average nodes $\bar{N}$ ranges up to 6500 in the LoRaWAN network transmitting a data message with FRM Payload of 30 byte. Note that the 1% duty-cycle limitation dominates the attribute of the network. The red dots are the optimized N_i, which is listed in Table 13.

As expected, higher SF contributes to less energy efficiency as compared to lower SF. Since ToA grows exponentially for the adequately delivering of a data message from end-device to gateway while reducing bit rate with each spreading factor. However, receiver sensitivity increases with advancing spreading factor, consequently enable higher coverage area for the LoRaWAN network. Therefore, it is an optimal approach to operate more nodes in lower SFs for better utilization of energy resources and also helps to make autonomous sensor network an energy efficient network.
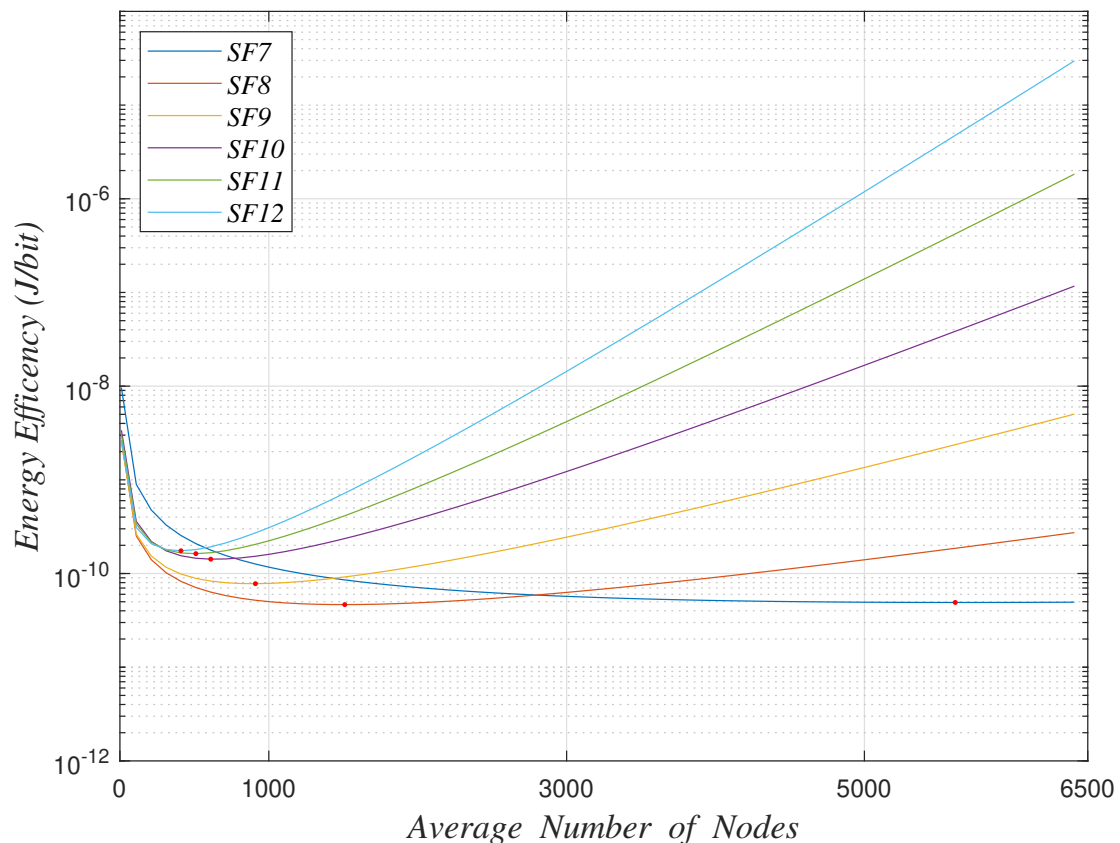
Figure 16. Energy Efficiency as a function of average number of nodes in each SF N_i.

In this work, we define energy efficiency in (30) as the average energy consumed per device; therefore, when minimized, it provides the maximum number of devices that the network can accommodate for given average energy consumption, which is exemplified in Figure 16. Notice that the crossing of $SF7$, $SF8$, and $SF9$ constitute an interesting

situation where the network operator has an opportunity to choose among the relevant spreading factors depending on the network application and also to make transmission network energy efficient at the same time. For instance, an average number of nodes up to 1510 would be feasible to be operated with $SF8$ having a medium coverage area with a good bit rate for sending data message from end-device to gateway.

Table 13 summarizes the optimal number of nodes in each SF to perform its operations competently while considering large dense LoRaWAN network engaging an average number of nodes $\bar{N}$ up to 6500. The optimal number N_i is listed since the distribution of end-devices based on SF has a high reliance on the specific IoT application. For instance, fast transmission in less coverage area, the LoRaWAN network will be more energy efficient when nodes communicate with lower spreading factor.

Table 13. Optimal Number of Nodes in each SF

DR	SF	Optimal N_i
5	7	5610
4	8	1510
3	9	910
2	10	610
1	11	510
0	12	410

The time-on-air (ToA) increasing exponentially with SF results in less energy cost of the LoRaWAN with a lower spreading factor. Furthermore, each spreading factor tends to approach optimized N_i, which gives an upper bound for a number of nodes to perform operations efficiently with less energy consumption.

5 CONCLUSION

Energy consumption is one of the objective compulsion in the process of designing and development of sensor network. In this research work, the energy consumption of Class A end-devices model has been presented for dense LoRaWAN network considering the data messages transmitted at regular intervals among nodes and gateways in confirmed and unconfirmed transmission. Average power consumption, energy cost, the lifetime of the sensor node, and energy efficiency are principle performance parameters that are dependent on the SF, frame payload size, and average coverage probability.

We presented through numerical results that the average power consumption in acknowledged and unacknowledged transmission inclines towards the sleep current when notification time grows since most often end-device is in the sleep state. Collision among transmitted signals from concurrently communicating nodes in dense LoRa networks is detrimental to the entire performance, which increases with an average number of nodes.

A sensor node operating on 2400 mAh battery transmits one message to gateway every 100 min with the higher spreading factor can have a theoretical lifetime up to 2.78 years as compared to 4.4 years for lower SF. Time-on-Air (ToA) and the number of nodes in each annulus are the main contributions of the overall energy cost of end-devices who exploit the characteristics of each SF. Finally, the energy efficiency of the LoRaWAN network is studied with respect to the distinct average number of nodes. The optimized number of nodes in each SF N_i and their respective energy efficiency level is presented. Furthermore, we demonstrated the superiority of lower over higher spreading factor in terms of energy efficiency over a circular coverage area having a radius of 3.6 km.

6 REFERENCES

[1] Chen S., Xu H., Liu D., Hu B. & Wang H. (2014) A Vision of IoT: Applications, Challenges, and Opportunities With China Perspective. IEEE Internet of Things Journal 1, pp. 349–359.

[2] Sisinni E., Saifullah A., Han S., Jennehag U. & Gidlund M. (2018) Industrial Internet of Things: Challenges, Opportunities, and Directions. IEEE Transactions on Industrial Informatics 14, pp. 4724–4734.

[3] Sotres P., Lanza J., Sánchez L., Santana J.R., López C. & Muñoz L. (2019) Breaking Vendors and City Locks through a Semantic-enabled Global Interoperable Internet-of-Things System: A Smart Parking Case. Sensors 19. URL: `https://www.mdpi.com/1424-8220/19/2/229`.

[4] Rodrigues J.J.P.C., De Rezende Segundo D.B., Junqueira H.A., Sabino M.H., Prince R.M., Al-Muhtadi J. & De Albuquerque V.H.C. (2018) Enabling Technologies for the Internet of Health Things. IEEE Access 6, pp. 13129–13141.

[5] Asadullah M. & Ullah K. (2017) Smart home automation system using bluetooth technology. In: 2017 International Conference on Innovations in Electrical Engineering and Computational Technologies (ICIEECT), pp. 1–6.

[6] Internet of Things (IoT) Connected Devices Installed Base Worldwide from 2015 to 2025 (in Billions), (accessed 16.10.2019). URL: `https://www.statista.com`.

[7] Sinha R.S., Wei Y. & Hwang S.H. (2017) A survey on LPWA technology: LoRa and NB-IoT. ICT Express 3, pp. 14 – 21. URL: `http://www.sciencedirect.com/science/article/pii/S2405959517300061`.

[8] Raza U., Kulkarni P. & Sooriyabandara M. (2017) Low Power Wide Area Networks: An Overview. IEEE Communications Surveys Tutorials 19, pp. 855–873.

[9] European Telecommunication Standard Institute (ETSI). URL: `https://www.etsi.org/`.

[10] Institute of Electrical and Electronics Engineering (IEEE). URL: `https://www.ieee.org/`.

[11] GSMA, Mobile internet of things: low power wide area connectivity. URL: `https://bit.ly/2Soue2F`.

[12] Lauridsen M., Vejlgaard B., Kovacs I.Z., Nguyen H. & Mogensen P. (2017) Interference Measurements in the European 868 MHz ISM Band with Focus on LoRa and SigFox. In: 2017 IEEE Wireless Communications and Networking Conference (WCNC), pp. 1–6.

[13] Burns J., Kirtay S. & Marks P. (2015) Future use of licence exempt radio spectrum. Tech. rep., Plum Consulting, Tech. (accessed on 01.03.2020). URL: `https://bit.ly/2Ixgdt5`.

[14] Mwakwata C.B., Malik H., Mahtab Alam M., Le Moullec Y., Parand S. & Mumtaz S. (2019) Narrowband Internet of Things (NB-IoT): From Physical (PHY) and Media Access Control (MAC) Layers Perspectives. Sensors 19. URL: `https://www.mdpi.com/1424-8220/19/11/2613`.

[15] Wang Y..E., Lin X., Adhikary A., Grovlen A., Sui Y., Blankenship Y., Bergman J. & Razaghi H.S. (2017) A Primer on 3GPP Narrowband Internet of Things. IEEE Communications Magazine 55, pp. 117–123.

[16] Petajajarvi J., Mikhaylov K., Roivainen A., Hanninen T. & Pettissalo M. (2015) On the coverage of LPWANs: range evaluation and channel attenuation model for LoRa technology. In: 2015 14th International Conference on ITS Telecommunications (ITST), pp. 55–59.

[17] Oh S. & Shin J. (2017) An Efficient Small Data Transmission Scheme in the 3GPP NB-IoT System. IEEE Communications Letters 21, pp. 660–663.

[18] Lora World Coverage, (accessed 04.03.2020). URL: `https://lora-alliance.org/`.

[19] GSMA, Security Features of LTE-M and NB-IoT Networks. URL: `https://www.gsma.com/iot/wp-content/uploads/2019/09/Security-Features-of-LTE-M-and-NB-IoT-Networks.pdf`.

[20] Cattani M., Boano C.A. & Römer K. (2017) An Experimental Evaluation of the Reliability of LoRa Long-Range Low-Power Wireless Communication. Journal of Sensor and Actuator Networks 6. URL: `https://www.mdpi.com/2224-2708/6/2/7`.

[21] An1200.22 LoRaTM Modulation Basics, Rev. 2. Semtech, 2015, (accessed on 17.09.2019). URL: `http://www.semtech.com/uploads/documents/an1200.22.pdf`.

[22] Augustin A., Yi J., Clausen T. & Townsley W.M. (2016) A Study of LoRa: Long Range & Low Power Networks for the Internet of Things. Sensors 16. URL: `https://www.mdpi.com/1424-8220/16/9/1466`.

[23] Lorawan Multitech mDot, (accessed on 01.11.2019). URL: `http://www.multitech.com/documents/publications/datasheets/86002178.pdf`.

[24] Hoeller A., Souza R.D., Alcaraz López O.L., Alves H., de Noronha Neto M. & Brante G. (2018) Analysis and Performance Optimization of LoRa Networks With Time and Antenna Diversity. IEEE Access 6, pp. 32820–32829.

[25] de Carvalho Silva J., Rodrigues J.J.P.C., Alberti A.M., Solic P. & Aquino A.L.L. (2017) Lorawan — A low power WAN protocol for Internet of Things: A review and opportunities. In: 2017 2nd International Multidisciplinary Conference on Computer and Energy Science (SpliTech), pp. 1–6.

[26] Phung K., Tran H., Nguyen Q., Huong T.T. & Nguyen T. (2018) Analysis and assessment of LoRaWAN. In: 2018 2nd International Conference on Recent Advances in Signal Processing, Telecommunications Computing (SigTelCom), pp. 241–246.

[27] Pötsch A. & Haslhofer F. (2017) Practical limitations for deployment of lora gateways. In: 2017 IEEE International Workshop on Measurement and Networking (M N), pp. 1–6.

[28] Cuomo F., Campo M., Caponi A., Bianchi G., Rossini G. & Pisani P. (2017) Explora: Extending the performance of LoRa by suitable spreading factor allocations. In: 2017 IEEE 13th International Conference on Wireless and Mobile Computing, Networking and Communications (WiMob), pp. 1–8.

[29] Casals L., Mir B., Vidal R. & Gomez C. (2017) Modeling the Energy Performance of LoRaWAN. Sensors 17. URL: `https://www.mdpi.com/1424-8220/17/10/2364`.

[30] Lora Alliance Technical committee. LoRaWAN^{TM}1.0.3 Regional Parameters, 2018, (accessed on 05.01.2020).

[31] Lora Alliance Technical committee. LoRaWAN^{TM}1.0.2 Regional Parameters, LoRa Alliance Technical Committee: San Ramon, CA, USA, 2017, (accessed on 13.11.2019).

[32] Haxhibeqiri J., De Poorter E., Moerman I. & Hoebeke J. (2018) A Survey of LoRaWAN for IoT: From Technology to Application. Sensors 18. URL: `https://www.mdpi.com/1424-8220/18/11/3995`.

[33] Asad Ullah M., Iqbal J., Hoeller A., Souza R.D. & Alves H. (2019) K-means Spreading Factor Allocation for Large-Scale LoRa Networks. Sensors 19. URL: `https://www.mdpi.com/1424-8220/19/21/4723`.

[34] Mikhaylov K., Juha Petaejaejaervi . & Haenninen T. (2016) Analysis of Capacity and Scalability of the LoRa Low Power Wide Area Network Technology. In: European Wireless 2016; 22th European Wireless Conference, pp. 1–6.

[35] [r5]. podere campáz - produzioni biologiche. (accessed on 15.05.2020).

[36] Codeluppi G., Cilfone A., Davoli L. & Ferrari G. (2020) Lorafarm: A lorawan-based smart farming modular iot architecture. Sensors 20. URL: `https://www.mdpi.com/1424-8220/20/7/2028`.

[37] Shuguang Cui, Goldsmith A.J. & Bahai A. (2004) Energy-efficiency of MIMO and cooperative MIMO techniques in sensor networks. IEEE Journal on Selected Areas in Communications 22, pp. 1089–1098.

[38] Paulraj A., Nabar R. & Gore D. (2008) Introduction to Space-Time Wireless Communications. Cambridge University Press, USA, 1st ed.

[39] Terrasson G., Llaria A. & Briand R. (2014) System level dimensioning of low power biomedical Body Sensor Networks. In: 2014 IEEE Faible Tension Faible Consommation, pp. 1–4.

[40] Terrasson G., Briand R., Basrour S. & Dupé V. (2009) A top-down approach for the design of low-power microsensor nodes for wireless sensor network. In: 2009 Forum on Specification Design Languages (FDL), pp. 1–6.

[41] Cheong P.S., Bergs J., Hawinkel C. & Famaey J. (2017) Comparison of LoRaWAN classes and their power consumption. In: 2017 IEEE Symposium on Communications and Vehicular Technology (SCVT), pp. 1–6.

[42] Kim B. & Hwang K.i. (2017) Cooperative Downlink Listening for Low-Power Long-Range Wide-Area Network. Sustainability 9. URL: `https://www.mdpi.com/2071-1050/9/4/627`.

[43] Sartori D. & Brunelli D. (2016) A smart sensor for precision agriculture powered by microbial fuel cells. In: 2016 IEEE Sensors Applications Symposium (SAS), pp. 1–6.

[44] Georgiou O. & Raza U. (2017) Low Power Wide Area Network Analysis: Can LoRa Scale? IEEE Wireless Communications Letters 6, pp. 162–165.

[45] Neumann P., Montavont J. & Noël T. (2016) Indoor deployment of low-power wide area networks (LPWAN): A LoRaWAN case study. In: 2016 IEEE 12th International Conference on Wireless and Mobile Computing, Networking and Communications (WiMob), pp. 1–8.

[46] Mikhaylov K. & Petäjäjärvi J. (2017) Design and Implementation of The Plug&Play Enabled Flexible Modular Wireless Sensor and Actuator Network Platform. Asian Journal of Control 19, pp. 1392–1412. URL: `https://onlinelibrary.wiley.com/doi/abs/10.1002/asjc.1492`.

[47] Gaelens J., Van Torre P., Verhaevert J. & Rogier H. (2017) Lora Mobile-To-Base-Station Channel Characterization in the Antarctic. Sensors 17. URL: `https://www.mdpi.com/1424-8220/17/8/1903`.

[48] Mahmood A., Sisinni E., Guntupalli L., Rondon R., Hassan S.A. & Gidlund M. (2019) Scalability Analysis of a LoRa Network Under Imperfect Orthogonality. IEEE Transactions on Industrial Informatics 15, pp. 1425–1436.

[49] Abramson N. (1970) The ALOHA SYSTEM: Another Alternative for Computer Communications. In: Proceedings of the November 17-19, 1970, Fall Joint Computer Conference, AFIPS '70 (Fall), Association for Computing Machinery, New York, NY, USA, p. 281–285. URL: `https://doi.org/10.1145/1478462.1478502`.

[50] Goursaud C. & Gorce J.M. (2015) Dedicated networks for IoT : PHY / MAC state of the art and challenges. EAI endorsed transactions on Internet of Things URL: `https://hal.archives-ouvertes.fr/hal-01231221`.

[51] Semtech Corporation SX1272/3/6/7/8: LoRa Modem. Designer's Guide. AN1200.13, Semtech Corporation: Camarillo, CA, USA, 2013, (accessed on 15.11.2019).

[52] Semtech SX1272, (accessed on 01.11.2019). URL: `http://www.semtech.com/images/datasheet/sx1272.pdf`.